USING MOTOR ELECTRICAL SIGNATURE ANALYSIS TO DETERMINE THE MECHANICAL CONDITION OF VANE-AXIAL FANS

Donald Scott Doan, B.S.

Thesis Prepared for the Degree of

MASTER OF SCIENCE

UNIVERSITY OF NORTH TEXAS

May 2002

APPROVED:

Mitty C. Plummer, Major Professor
Philip R. Foster, Committee Member
J. Lynn Johnson, Committee Member
Daniel N. Hopkins, Industrial Representative, Principal Engineer, TXU
Albert B. Grubbs, Chair of the Department of Engineering Technology
C. Neal Tate, Dean of the Robert B. Toulouse School of Graduate Studies

Doan, Donald Scott, Using Motor Electrical Signature Analysis to Determine the Mechanical Condition of Vane-Axial Fans. Master of Science in Engineering Technology, May 2002, 112 pp., 12 tables, 32 illustrations, and 32 references.

The purpose of this research was a proof of concept using a fan motor stator as transducer to monitor motor rotor and attached axial fan for mechanical motion. The proof was to determine whether bearing faults and fan imbalances could be detected in vane-axial fans using Motor Electrical Signature Analysis (MESA).

The data was statistically analyzed to determine if the MESA systems could distinguish between baseline conditions and discrete fault frequencies for the three test conditions: bearing inner race defect, bearing outer race defect, and fan imbalance. The statistical conclusions for these proofs of concept were that MESA could identify all three faulted conditions.

ACKNOWLEDGMENTS

I would like to acknowledge and express my gratitude to my advisor and major professor, Dr. Mitty Plummer. His guidance and support in counseling me through this project and the research process were invaluable.

I would like to thank my committee members, Dr. Phillip Foster and Dr. Lynn Johnson for their support of this project and the time they spent reviewing my thesis. I would especially like to acknowledge my Industrial Representative, Dr. Dan Hopkins. In addition, I would like to extent my gratitude to industrial teams:

Mr. Noah Bethel of PdMA for the use of the PdMA system for Motor Current Demodulation testing; Dr. Ernesto Wiedenbrug of Baker Instruments Inc. for the use of their system for Instantaneous Torque; and Brian Rucker of SWANTECH, LLC for the use of the Shock Pulse Monitoring System. Without the support of these vendors and their commitment to this research, this project would not have been realized.

I express my sincere gratitude to Mr. Henry Carr and his staff at TXU Generation for assisting me with the testing and configuration changes to the test fan. I would also like to thank to Operations Smart Team 3 for their support of this project. Finally, I wish to thank Ms. Pamela Fuller for the many hours she spent helping me proofread the drafts of this thesis.

TABLE OF CONTENTS

LIST OF TABLES

LIST OF ILLUSTRATIONS

Figure Page

CHAPTER 1

INTRODUCTION

Vane axial fans supply and exhaust air at higher pressures and at greater flow rates than squirrel cage fans and so find frequent applications in the nuclear power industry In the nuclear power industry, failure of these fans can result in unplanned outages, health and safety costs, maintenance costs, and extensive damage to ancillary equipment. (Electric Power Research Institute, 2001). In particular, the incipient failures of the rotating components before the analyzed end-of-life require considerable maintenance in nuclear power plants (Electric Power Research Institute, 1991).

Vane axial fans take the form of horizontal mounted and vertical mounted fans. These fans are typically mounted in the air stream and use either direct drive or belt drive systems. The installations at most nuclear power plants are direct driven fans, which have the motor in the air stream, close coupled to the fan, and mounted to the air ducting through diffusers on one end and a support plate or rods at the other end (Figure 1) (Aerovent 1991).

This arrangement presents a barrier to applying predictive maintenance tools to monitor the condition of the motor and fan rotating components. The best method of detecting anti-friction bearing failures (rolling element bearings) is by attaching an accelerometer to the bearing housing on or near the load zone of the bearing (Shock & Vibration Handbook, 1988).

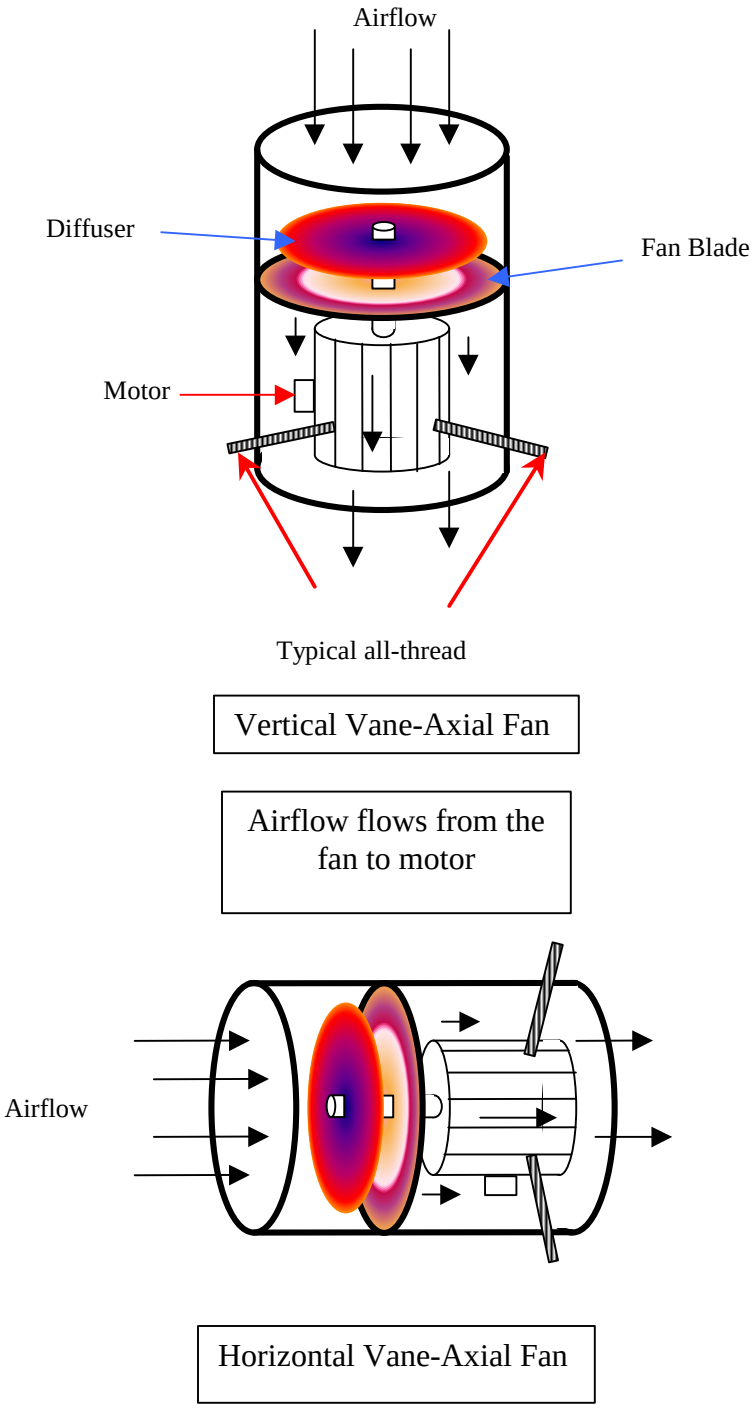

Figure 1. Typical Direct Drive Vane-axial Fans (Aerovent Products, 1996).

It is difficult to detect failure modes in vane-axial fans. Damage to the rotating equipment due to incipient failures can cause secondary failures or ancillary failures of component trains (Mitchell, 1993). A good condition based maintenance program designed from a failure modes and effects analysis basis determines the type of technology to apply to assist in detecting the failure modes (Berry, 1993). Good installation and lubrication practices during manufacturing and rebuilding of rotating equipment reduce the probability of component incipient failures but do not eliminate them. The ability to detect failure modes and plan maintenance is the purpose of a reliability centered maintenance concept (Mitchell, 1993).

Figure 2. Typical Horizontal Direct Drive Vane-axial Fan Installation (Comanche Peak Steam Electric Station, TXU Electric, CPSES).

The field of condition-based maintenance continues to advance and refine in step with the advances in digital technology (Harris, 1988). In the last few years, a new method of detecting rotating component failure modes was developed from research conducted at the Oak Ridge National Laboratories (Casada, 2001). This method uses the stator of an induction motor as a transducer to measure mechanical influences affecting the rotor (Casada, 1999). The significance of this technology is the ability to detect changes in torque and analyze the motor current data. Where the use of filters and digital signal processing is employed to analyze the signal for processes that could affect the instantaneous electrical signal (Casada, 1999). Using the motor stator as a transducer enables the measurement of mechanical responses. When the vibration data quality does not provide enough information to detect incipient failures, this new technology is available to apply to the failure mode and effects analysis (Bethel, 2001).

Vane-axial fans bearing failures, rotor misalignment, and rotor imbalance present a challenge to predictive techniques, which for incipient failures, is detectable using bearing housing vibration. The current method of taking cowling vibration and trying to determine bearing housing defections caused by mechanical transients is not adequate (Riley, 1997). Very little of the rotor energy is transmitted to the surface through the bearings, bearing housing, and motor support system to the cowling. With this transmission path, the signal-to-noise level is very small and the bearing fault frequencies are lost in the noise. Therefore, the advent of electrical motor current analysis with advanced digital technology should assist in the detection of vane-axial fan rotor mechanical conditions (Wiedenurg, 2001).

Figure 3. Typical Vertical Direct Drive Vane-axial Fan (CPSES).

Figure 4. Typical Vertical Direct Drive Vane-axial Fan in operation. (CPSES).

Figures 2, 3, & 4 are pictures of vane-axial fans installed at Comanche Peak Steam Electric Station, TXU Electric in Glen Rose, Texas. They illustrate the horizontal and vertical orientation of the fan in the ventilation systems.

Problem Statement

The problem addressed in this research is the comparison of Motor Electrical Signature Analysis to the mechanical vibrational data collected on the bearing housings. The motor used in this research is attached to an Airoflow vane-axial fan. This type of fan is the most common exhaust fan used at CPSES and throughout TXU (Gastonal, 2001). Motor Electrical Signature Analysis is used within TXU to determine the condition of the motor stator and rotor with spectral analysis of the current signature.

The current method of measuring motor mechanical vibration and equating that vibration to an actual fault mode of the rotating system is inadequate (Baxter, 2001). The transmission path for the vibration signal is attenuated due to the tortuous path from the initiating event to the fan housing. This attenuation causes the signal-to-noise ratio to decrease to a differential that makes it difficult to extract rotating dynamic data from the signature. The vibration signature is dominated by the vane airflow noise over the diffuser and fan blades in the air stream. This airflow noise can exceed the base signal level by over 90 decibels.

Purpose

The purpose of this research is to determine if Motor Electrical Signature Analysis can identify vane-axial fan rotating equipment mechanical vibration signatures that indicate faults, and if the Motor Electrical Signature Analyses are equivalent in sensitivity to those from vibration transducers mounted on the bearing housings.

Research Questions

There were two research questions addressed by this thesis. The first research question deals with the Motor Electrical Signature Analysis of bearing defect frequencies:

1. Will the use of cowling mechanical vibration detect rotating system faults in the motor rotor system compared to the bearing housing mechanical vibration?

This question has a corresponding null hypothesis 1 $(H_o)_1$: there is no difference between the change in the mechanical signature on the cowling and the change in the baseline mechanical signature on the bearings housing. This is represented by equation 1 below where μ is the population of data collected for this comparative test.

$$\mu_{\text{diff (cowling - baseline)}} = 0 \qquad (1)$$

This question has an alternative hypothesis 2 $(H_a)_1$: the difference between cowling population and the bearing population is greater than zero. This is represented by equation 2.

$$\mu_{\text{dif (cowling - baseline)}} > 0 \qquad (2)$$

The second research question deals with the Motor Electrical Signature Analysis and rotor eccentricity and the effects on the motor bearing and the motor electrical signature.

2. Will the use of Motor Electrical Signature Analysis detect changes in magnitude indicated by amplitudes of the frequencies produced by rotating equipment faults?

This question has a corresponding null hypothesis 2 $(H_o)_2$: there is no difference between the change in the electrical signature and the change in the baseline mechanical signature on the bearings housing due to rotating equipment faults. This is represented by equation 3 below where μ is the population of data collected for this comparative test.

$$\mu_{\text{dif (MCSA-baseline)}} = 0 \tag{3}$$

This question has an alternate hypothesis 2 $(H_a)_2$: there is an increase in the motor electrical signature analysis running speed spectra and the baseline bearing casing spectral data. This is represented by equation 4.

$$\mu_{\text{dif (MCSA imbalance-baseline imbalance)}} > 0 \tag{4}$$

Assumptions

The following assumptions applied to the research performed in the test and comparison phase of this thesis:

1. The measuring and test equipment used in this research were assumed to provide accurate measurements because the systems used were compared to a calibrated system that is traceable to the national standards (Appendix D). The systems used in the comparison were received and operated by the companies sponsoring the systems.
2. The fan system used in this research was a new fan assembly removed from the CPSES warehouse for this test. The fan is a typical fan used in exhaust systems at CPSES. The support system for the fan is an internal frame welded to the cowling (ducting), and differs from Joy axial-vane fans. This difference does not affect the quality of the vibration measurements on the fan cowling.
3. All the bearings were new and unused; therefore, the bearing quality was assumed to be within manufacturing tolerances.
4. The test stand used in the running of the motor does not affect the rotor dynamics of the fan system.
5. Installation techniques were consistent with the techniques used in the field.
6. The data collection techniques are consistent with the collection techniques used in the field.
7. The supply power was of a quality that would not interfere with the motor electrical signal data collection.

Limitations

This research had the following limitations:

1. The test was performed on one type of motor application.
2. One test fan was used.
3. The test was performed at ambient temperature and humidity.
4. The test was performed at the same barometric pressure.
5. No known mechanical faults were present that could skew the data.
6. Testing was performed at TXU's Smart Team Three test facilities.

Terminology

1. CPSES – Comanche Peak Steam Electric Station, TXU Electric
2. BPIR – Ball Pass Inner Race
3. BPOR – Ball Pass Outer Race
4. DFLL – Digital Frequency Locked Loop
5. MESA – Motor Electrical Signature Analysis
6. EPRI – Electric Power Research Institute
7. FFT – Fast Fourier Transform
8. ORNL – Oakridge National Laboratory
9. TXU – The name of the parent utility for Comanche Peak Steam Electric Station

Overview of the Remainder of the Research

Chapter 2 provides a review of literature related to the thesis. Specifically discussed are the motor current demodulation, instantaneous torque motor electrical signature analysis, and vibration analysis as it applies to this research. Chapter 2 concludes with a review of literature for the basis of motor electrical signature analysis in the nuclear industry, and related research.

Chapter 3 provides the details of the research including research design, control of variables, sample selection and treatment, test equipment, and testing methodology. The statistical basis for this research including sample size and objective criteria is also provided.

Chapter 4 contains the testing results and the analysis as well as the observations made during the testing. The conclusions reached from this research are discussed in Chapter 5. Chapter 5 also contains recommendations for further research.

CHAPTER 2

REVIEW OF LITERATURE

The review of literature focused primarily on: MESA, vibration signal analysis, stress wave analysis, and the dynamics in a rolling element bearing support system. Any relevant research related to this topic at TXU or that dealt with the measurement of motor electrical signal to detect rotor dynamics was reviewed.

Motor Electrical Review

The Electric Power Research Institute (EPRI) provides background information on electrical motor fundamentals (EPRI 1991). According to the EPRI reference, there are many different types of motors in use in the electric power industry. The poly-phase induction motors are used to provide good starting torque and running torque characteristics for a variety of applications within the power plants. Because bearings are the primary cause of motor failure, proper maintenance and monitoring are a primary concern of plant engineers and maintenance personnel.

In the circuit analysis of squirrel cage induction motors there are two types of circuits: approximate and exact versions. No truly "exact" circuit exists. The reason is that the electromagnetic components are non-linear due to the interactions between the coils of wire and magnetic core. The motor windings exhibit no direct linear relationship between applied voltage and current.

A second shortcoming of the equivalent circuit is its use of lumped or discrete circuit elements, such as a single value of inductance to represent what is actually a

distributed value. That is, a coil in the motor does not exhibit an inductance and resistance for the entire length, but each length has its own resistance and inductance.

These two items, lumped / discrete components and non-linear characteristics of induction motors, inhibit the ability to use the motor stator as a transducer for the mechanical characteristics of the rotor. With the complexity of each motor and the non-linear quantities, a method of detecting rotor ailments using the stator was limited to rotor bar issues and eccentricity between the rotor and stator (Casada, 1999).

When first evaluating a motor, the first method of data research is the nameplate method. This is the most trivial and least intrusive, and in consequence usually the least accurate. The motor ratings: efficiency, insulation class of winding, horsepower, current draw, voltage, and service factor are listed on the nameplate. It is unlikely that the machine will perform at the nominal efficiency. Load variations, as well as the non-linearity of the motor along with source imbalances and harmonic components change the efficiency. The nameplate is derived from a statistical evaluation of a class of motors and does not necessarily coincide with the particular motor under observation (Wiedenbrug, 1998).

The electrical qualities of the motor are influenced by allowable manufacturing tolerances, and the specifications allow for error in the nameplate data. NEMA specifies up to 20% of error for the nameplate slip, and error in the rated current may be as large as 10% on a healthy induction motor, according to NEMA (Wiedenbrug, 1998).

The equivalent circuit is used to determine the characteristics of an induction motor. Figure 5 shows the basic per phase equivalent circuit for an induction motor.

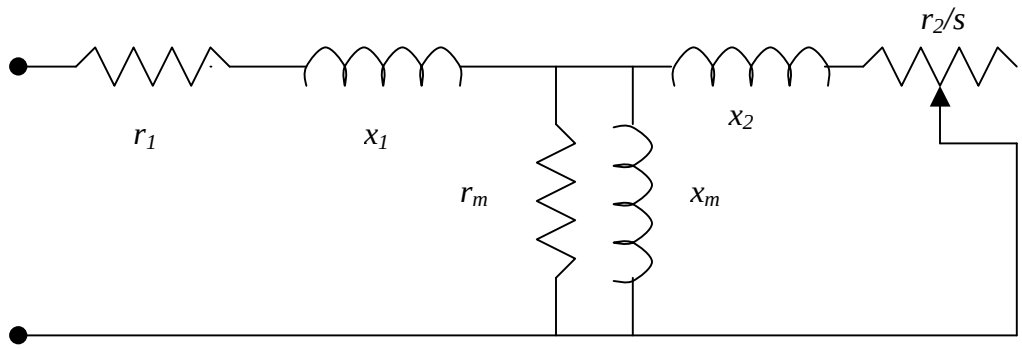

Figure 5. The Equivalent Circuit for an Induction Motor (Wiendenbrüg, 1995).

From Figure 5, r_m and r_1 respectively represent the stator and equivalent rotor resistances, x_m and x_1 the leakage inductances for the stator and referred rotor, x_m the mutual or magnetization inductance, r_0 models the core losses, and s represents the slip of the given operating condition. (See equation (5).

$$S = \frac{synchronous(rpm) - actual(rpm)}{synchronous(rpm)} \qquad (5)$$

This model's disadvantages are that the harmonics and imbalances are not accounted for, and the friction and windage values must be estimated because they are not observable. These characteristics are necessary to help determine the quality of the

signal and the measurable values that could be used in determining the rotor condition. The methods for the MESA have varied approaches (Wiedenbrug, 1998).

One method that Oak Ridge National Labs used was motor current demodulation. A team studying the motor current signatures (Motor Current Signature Analysis, MCSA) of Motor Operated Valves for the Nuclear Regulatory Commission in the early 1980's first perfected this method (Casada, 1999). The motor current demodulation grew out of the need to determine torque thrust of motor operated valves due to an increasing number of incidents in the nuclear industry of valve seat failures from over-torquing. Most Motor Operated Valves (MOV) motors are only energized for a minute or less during an open or close command. The circuits are usually equipped with a torque switch, which stops the motor from binding the valve disk to seat or other components. With the short duration run time of the MOV, traditional vibration analysis methods were ineffective in predicting the torque to which the MOV's were subjected, leading to the over torquing of the valves (Casada, 1999).

The development of instantaneous torque from the motor current grew out of electrical current analysis for rotor bar and eccentricity measurements that date back to the advent of swept filters and oscilloscopes. The systems were used to determine pole passing frequencies and air gap issues with squirrel cage induction motors. The torque curve was developed from demodulated motor current signatures. The phase coined by the research team was Motor Current Signature Analysis (MCSA), which developed the method by using demodulation techniques to measure torque. It was found that the torque signature also included a signature profile that resembled the gear mesh between

the drive and the gear system that transmitted the torque developed by the motor to drive of the valve stem (Casada, 1999).

This was taken one step further by Oak Ridge National Laboratories to include the mechanical signature of rotating elements that would affect the instantaneous torque of the drive motor. These attributes included process variables including belts, pulleys, gears, and load changes on the motor shaft.

The idea to use Motor Current Signatures to measure mechanical signatures of the rotating system originated from the Motor Operated Valve research where the characteristics of an ideal transducer were recognized in the motor stator and rotor system. The ideal transducer would have a linearity of amplitude and phase, good frequency response, a large dynamic range, and accurate measurments. Motor stator and rotor system have these characteristics. The stator is the transducer that measures the power (voltage and current) used to create the magnetic flux to move the rotor. The stator's voltage and current can be measured indirectly through current and voltage transducers. A graph of these qualities are shown in Figure 6.

Typical current transducers are either clamp-on transformers or permanently installed on the load leads. The clamp-on transducers are either a self-generating current transformer or a Hall effect (current sensitive) semi-conductor measurement device. Voltage transducers are either portable direct reading voltage systems or permanently installed potential transformers that read either across two phases of an electrical system or between a phase and ground.

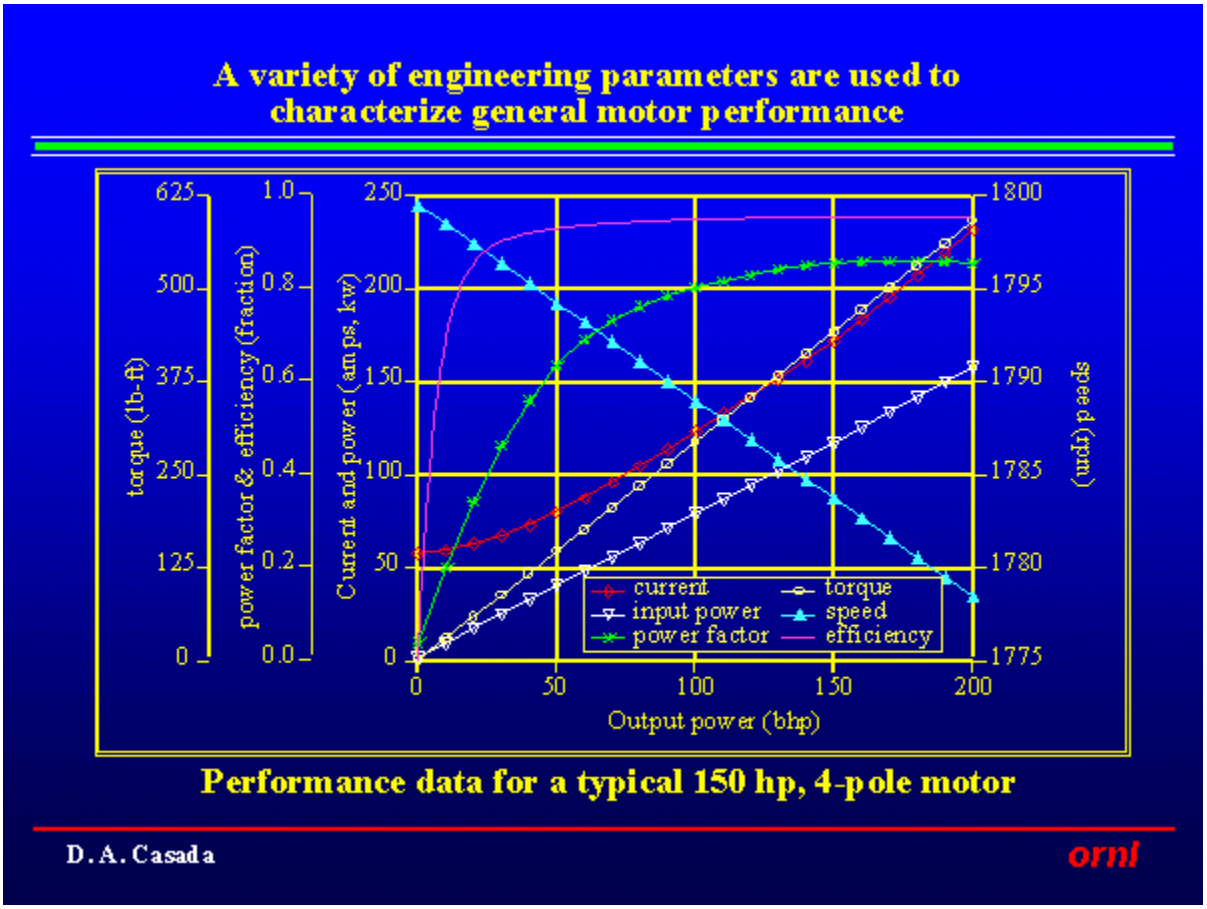

Figure 6. Motor Data for Typical Induction Motor (reprinted by permission – Casada, 1999).

The proceeding figure shows the electrical characteristics of a one hundred fifty horsepower induction motor. The vertical axis is broken into four (4) scales: torque, power factor, current / power, and speed. The horizontal axis is the amount of output power that is applied to the motor. This power is usually a function of the mechanical system's design (Casada, 1999). The curves are the different functions over the output power of the motor. Oakridge National Laborites used these curves to develop the first generation of Motor Current Signature Analysis (Casada, 1999).

The distribution system affects the operation of the motor and rotor system, and a change in the line voltage will change the load current.

$$I_s = \frac{Z_s}{V_T} \tag{6}$$

Where $I_s \rightarrow$ current of the stator

$Z_x \rightarrow$ impedance of the stator

$V_t \rightarrow$ terminal voltage

The AC voltage of the stator is the same voltage as the terminal voltage (V_T) and the stator current changes inversely with the terminal voltage. This will affect the overall impedance of the system by changing the magnetic coupling between the rotor and the stator (see description of equivalent circuit, page 14).

When these electrical variables are understood and accounted for, the use of a motor stator as a transducer to measure mechanical influences on the rotor along with digital signal processing becomes an alternative to traditional methods of measuring rotating equipment degradations (Gökmem, Eldem, Duyar, p. 1, 2001).

> Traditional failure prediction systems such as vibration based systems, often do not go beyond providing the measurements and tools to analyze and trend those measurements. The influence of external factors like external vibrations, the exact location of the measurements further complicate the issue. The expert systems that are used in large plants have their own limitations. They require an extended training period for the database to be built up, in order to work reliably. In addition, as time passes the database often will need to be updated as new incidents occurs. False alarms can become serious headaches with these systems. On the other hand, measurement of electrical signals such as voltage and current is much more reliable and easy, and the effects of several faults on stator current are well-known[1,2]. Mechanical faults such as air gap eccentricities, misalignment and ball bearing defects affect the permeance and electrical faults such as broken rotor bars have an effect on magnetomotive force. The quantities are directly related with stator currents.

This research into the use of stator current to determine the mechanical condition of the rotating systems is one of the aspects this research will try to correlate with mechanical vibration signature analysis. If these theories are proven to be practical in the measurement of vibration related phenomena on vane-axial fans, utilities and most manufacturing plants will have an inexpensive alternative to mounting sensors on motor and fan shrouds.

Motor Current Research, Oak Ridge National Laboratories

Using motor data to improve system reliability and reduce operating costs started as a research tool. It is now being used in limited applications in the utility, steel, and petrochemical industries. The original licensee of this technology is Lockheed Martin, the contractor operating Oak Ridge facilities for the Department of Energy, where the following described work originated (Casada, 1998).

The Motor Current Signal Analysis (MCSA) is a relatively new diagnostic field that can be used to supplement the existing condition-based techniques used to assess the "health" of motors and motor driven equipment. This MCSA began from studies by Dave Eissenberg and Howard Haynes during their research of motor-operated valves for the Nuclear Regulatory Commission (Casada, 1998). This technology is starting to be applied to more varied applications, other than motor-operated valves, and new research and advances are occurring in the area of on-line motor current analysis systems developed independently from the research performed at ORNL (Casada, 1998).

One problem area in new research is that there are no firm criteria for what level / amplitude / severity of a particular signal constitutes a problem with the machinery (Casada, 2001). In comparison to vibration data levels of severity that have been

developed over the years of research and application, the "Rules of Thumb" have not been uniformly adopted over the years. In the vibration domain as well as in this emerging technology, trending is a more important activity in condition monitoring (in most cases) than the absolute overall magnitude of the signal. This is due to difficulty of quantifying the setting of rigid severity levels (Casada, 2001).

The use of motors as a possible transducer has its appeal because over half of the electrical generation in the U.S.A. is used to drive induction motors. The cost of motor usage exceeds $ 90 billion per year, there are over 125 million motors in the 1 to 125 horsepower range used in industrial applications (Casada, 1998 & EPRI, 1991). With this large population of motors used in a multitude of different applications, the idea of developing the motor stator as a transducer is appealing for repeatability and quality of the reproduced signal (Casada, 2001).

The qualities of a good transducer are a good description of the stator rotor system of an induction motor. Not only is the linearity, frequency response, dynamic range, accuracy, and repeatability important during data collection, but it carries over to all steps in the signal processing. One variable that is hard to control during data collection on electrical equipment is the bus voltage variations. These variations in relation to the use of a motor as a transducer affect the current signal in the stator of the motor. These variances affect the current, but power is relatively stable since the power in an induction motor is controlled in large by the load (Casada, 1998).

The following Figures 7 and 8 depict how the changes in line voltage affect the instantaneous current and the instantaneous power in a typical induction motor. As the terminal voltage changes, the current used to produce the same power changes. The

voltage and current are inversely proportional: as the terminal voltage increases, the current decreases. In Figure 7, the bus voltage increase from 95% nominal to 100% nominal terminal voltage while the average current decreases from 119.5 amps to 114 amps.

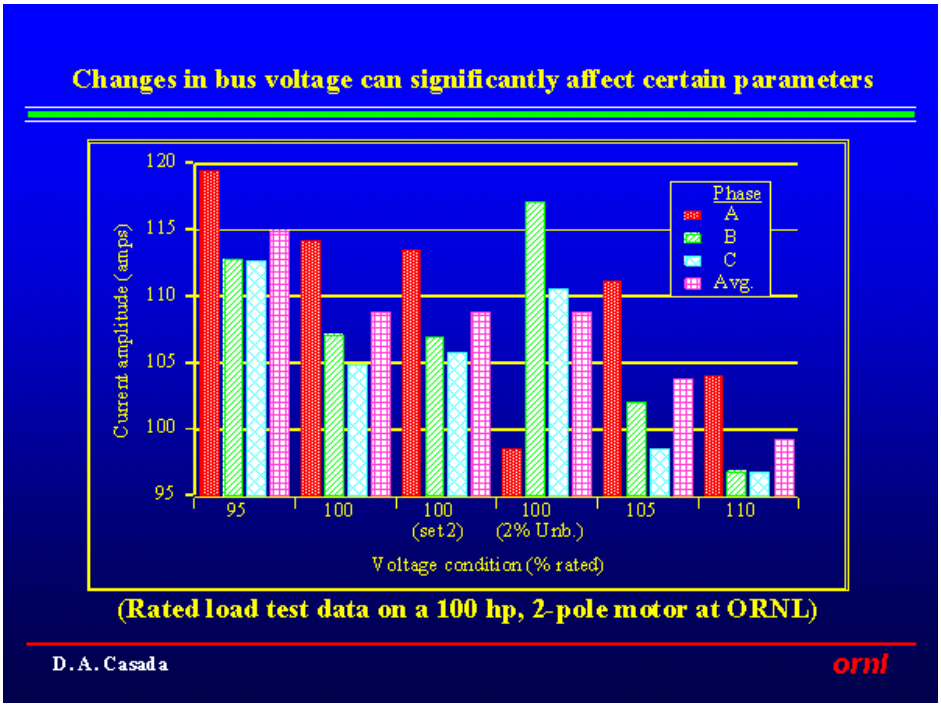

Figure 7. Changes in Bus Voltages Effect on Motor Current (Casada, 1998).

In Figure 8, the effect on the motor current is greater than the effect on total power of the system, since:

$$P_I = V_t * I_T (\cos q) \qquad (7)$$

P_I = input power
V_t = terminal voltage
I_T = total current
$(\cos q)$ = the cosine of the phase angle between voltage and current (power factor)

The change in terminal voltage does not appreciably change the total power used by the motor but does affect the current draw.

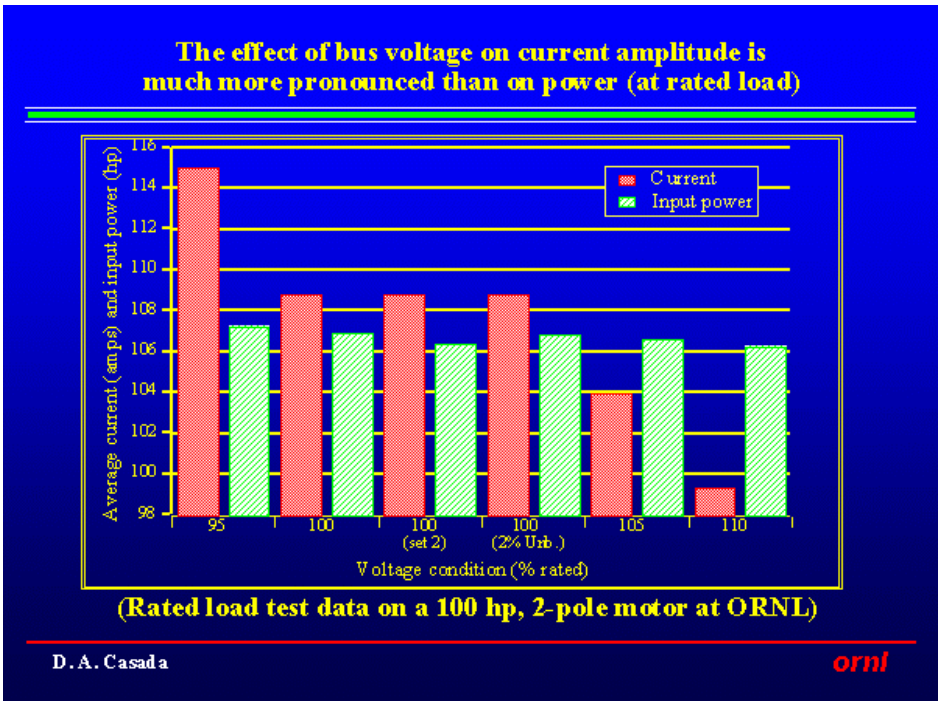

Figure 8. Relative Constant Power Consumption with Bus Voltage Changes (Casada, 1998).

Signal conditioning and the methods of processing the signal are important to the stator if it is used as a transducer. Some of the diagnostic tools used in the processing of the signal are broken into two distinct parts, demodulation and filtering. Demodulation of the signal can be either analog or digital. The analog demodulation does not significantly change the signal-to-noise ratio found in the original signal. Some digital demodulation techniques will decrease the signal-to-noise ratio depending on dynamic range of the processor and signal condition. The one area of improvement is the time saved in the CPU computation by analog demodulation. Other factors that come into play

in the demodulation of induction motor signals are the amplitude of the signal and phase relationship between the demodulated signal and the original (Casada, 1998).

The other part of the pre-processing prior to signal analysis is the filtering. The different methods used for demodulation of current signals, or any signal for that matter, is the use of low-pass for anti-aliasing, low frequency noise (DC) high-pass (Casada, 1998).

Demodulation of the current signal uses amplitude demodulation, which is the same as an AM radio demodulator. The carrier wave is the 60 Hz alternating current, after the current is demodulated. What is left is the signal due to varying load on the motor. Since line-voltage affects the quality of the AC current, care is needed to ensure line voltages are stable (Casada, 1998).

The following Figures 9 and 10 show an example of demodulating the AC current in a motor assuming constant line voltages. Without demodulating the AC current, it is almost impossible to differentiate the difference between a steady load signature and a fluctuating load signature. In Figure 9, the fluctuation load is the red-dotted line, while the steady load is the green line. There may be some phase difference with the peak current time varying, but the actual load changes are difficult to discern.

In Figure 10, the fluctuating load is once again the red-dotted line and the steady load is the green line. This figure shows how, in demodulation, the steady load has no current or phase variation over time whereas the fluctuation load current and phase varies periodically over time.

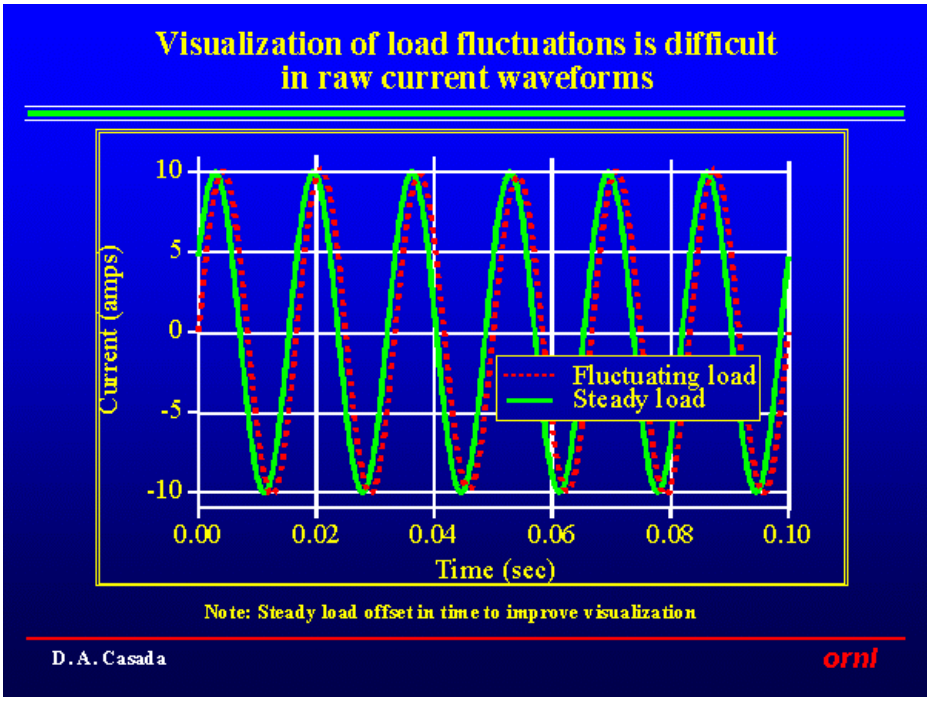

Figure 9. Steady Load and 15 Hz Fluctuating Load (Casada, 1999).

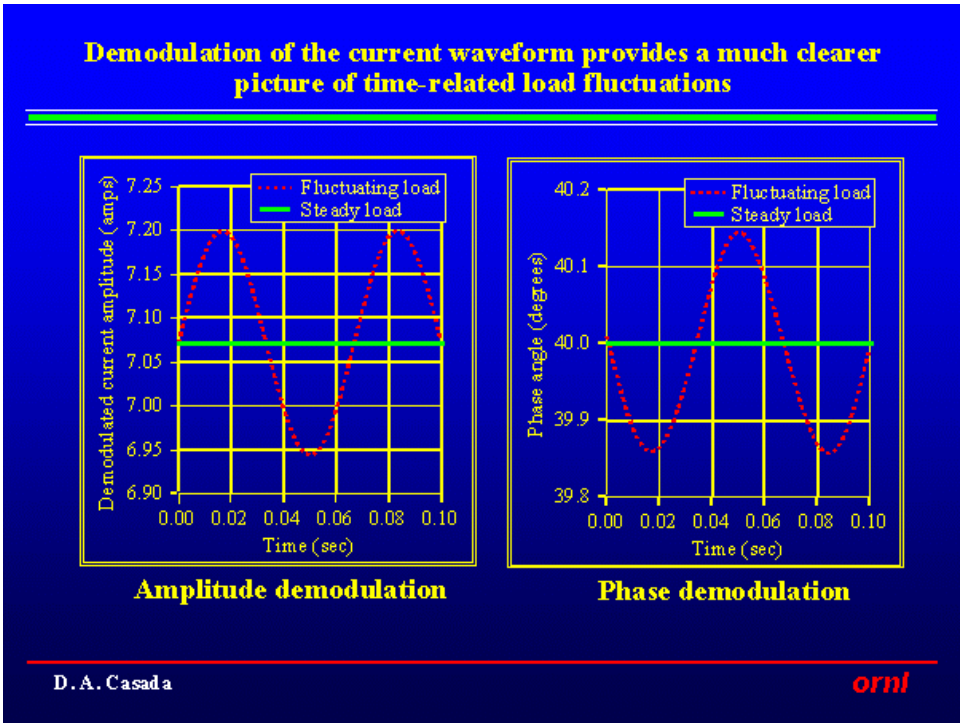

Figure 10. Demodulated Current for Steady Load and 15 Hz Fluctuating Load (Casada, 1999).

The previous Figures 9 and 10, depict the difference between demodulated and normal power flow in an electrical motor stator. The steady load when demodulated does not change periodically over time, where the fluctuating load does vary with time. Since the line supply voltage and current influence the steady load, demodulation removes this influence and leaves only the fluctuating load. This fluctuating load is due to imbalances, misalignment, or other physical effects that change the response of the rotor. When the signals are added together, the small fluctuation due to the varying load is lost in the 60 Hz signal (Casada, 1998).

Once the current signal is demodulated, the resultant time waveform is the variance in the load as seen by the stator. This variance, if voltage is stable, is due to the changes in load on the shaft. These load changes are the result of process changes, rubs on the rotor, misalignment of the rotor, belts, pulleys, and possible bearing effects. By measuring this demodulated current signal, it is possible to derive a time waveform that is representative of the mechanical influences on the rotor. This time waveform can further be analyzed with different types of transforms that return a frequency domain representation where the dominant frequencies can be trended to determine the condition of the rotating equipment's status (Casada, 1998).

The current demodulation process is applicable as long as line voltage does not vary. As mentioned earlier, another method of demodulation of the motor electrical signature is by using the power signature. The power signature is inherently demodulated by the cross product of the voltage and current. The resultant waveform is demodulated from the 60 Hz carrier frequency, but will contain two timeline frequencies and harmonics due to the multiplication of the two cosine waves. These harmonics can be

removed by using a low pass filter system (Casada, 2001). Later in this chapter, we will discuss the frequencies of concern in most AC induction motor's mechanical signatures and generation of these frequencies.

Another electrical characteristic used to measure the mechanical system response is the torque of the motor rotor as it is reflected into the stator across the airgap between the motor and the stator. The original research into motor current signature analysis was funded through Oak Ridge National Laboratory for the Nuclear Regulatory Commission for Motor Operated Valves (Casada, 1999). As mentioned earlier, the measurement of the instantaneous torque signature was developed for Motor Operated Valves. One method to derive a torque signature is from:

$$T_e = \left(\frac{3}{2}\right)\left(\frac{P}{2}\right)\left(\psi'_{qs} i'_{ds} - \psi'_{ds} i'_{qs}\right) \qquad (8)$$

Where:

T_e → Torque

P → Number of motor electrical poles

(ψ'_{qs}) → Linked flux quadrature

(ψ'_{ds}) → Linked flux dynamic

i_{ds} → Dynamic current

i_{qs} → Quadrature current

Equation (8) is used as the base for the algorithm used to develop the torque waveform in order to extract exact frequencies and magnitudes using Fast Fourier Transforms and digital frequency locked loop (Wiedenbrug, 1998). The linked flux values are from predetermined experimental values used by Dr. Wiedenbrug as estimates for the purpose of the torque conversion. The dynamic current is measured using

"clamp-on" transducers and the quadrature current is calculated from the linked flux calculations (Wiedenbrug, 1998).

The digital frequency locked loop (DFLL) is a wavelet function used to extract the exact frequencies of complex waveforms, such as the torque signal, in a short sample time. The advantage of DFLL is that the initial data collection time is quicker than the time requirement for FFT and spectrum functions. FFT's assume that the signal is of infinite duration in time and since the signal is not infinite, artifacts arise such as alias frequencies, sums and differences, etc. The wavelet has certain frequency components, while bundling its energy to a short duration in time. It is very important to note that it is not necessary to have a sinusoidal wave component for the wavelet to work. In induction motors, the sinusoidal wave can be used effectively to filter out certain frequencies from the spectrum (Wiedenbrug, 1998).

> An advantage of wavelet theory is that it allows joint time-frequency analysis. This approach enables observations of the frequency domain, while simultaneously seeing the time variation. This is achieved by creating the inner product of the family of wavelets, using inner frequency f_1 as the parameter that filters out the frequency. With this variable, a family of wavelets is created with:

$$j_1(t) = w(t) \cdot \sin(2p \cdot f_1 \cdot t) \tag{9}$$

$$w(z) = \frac{1}{2}(1 - \cos(2p \cdot f_1 \cdot t))_{z=0}^{z=1} \tag{10}$$

Where:

f_1 → Wavelet function
w → Window function
z → Proportional to time, ranging from 0 to 1
f_l → Inner frequency used to filter out specific frequencies
t → time

Equation 9 and 10, wavelet and window functions for DLL (Wiedenburg, 1998)

The wavelet theory is basically composed of two waveforms. The wavelet function is used to filter torque using the windowing function to extract the frequency domain amplitude and frequency as defined by the wavelet function. The wavelet function is tuned to a specific frequency, then it is passed through the instantaneous torque function which determines the frequency to within 0.001 Hz. This can be accomplished within a 10-second data acquisition. This is substantially quicker than using an FFT to capture data at the same resolution (Wiedenbrug, 1998).

Conversely, the FFT function is much slower at acquiring a high-resolution frequency peak. For the same frequency resolution of 0.001 Hz in a 1000 Hz band, the time to acquire the data is calculated by:

$$FFT\ \ time\ T = \frac{1}{\Delta f} \tag{11}$$

T → time

f → *frequency*

$$FFT\ \ time\ T = \frac{2^n}{2.56F_{\max}}\ or\ \frac{\#lines}{F_{\max}} \tag{12a}$$

For a resolution of 0.001 Hz at 10 Hz:

$$FFT \quad time \ T_b = \frac{10000}{10} = 1000 \text{ sec } @ \, 10 \, Hz \text{ max} \qquad (12b)$$

As can be seen in equation (12b), it takes 16.67 minutes to discern a frequency peak with 0.001 Hz resolution. This is two magnitudes longer that the DFLL. Even with the FFT being inherently slower in data acquisition, most of the signal processing problems have been identified with it. The DFLL is still a new algorithm and the signal processing problems are yet to be completely bounded (Wiedenbrug, 1998).

Technology Review

The two companies that assisted in this project each used different approaches in the analysis of the data collected using motor current analysis. PdMA used motor current demodulation and performed a high resolution FFT on the data collected. A high-resolution FFT of a demodulated current signal for high-resolution differential frequency has good noise-to-signal ratio. The higher the resolution, the less error or noise introduced due to leakage between ensembles of data. To improve the signal-to-noise ratio, the signal was sampled and averaged many times. This is one drawback of FFT analysis: the higher the quality of the FFT, the longer the data acquisition takes.

PdMA

PdMA developed a tester that uses amplitude demodulation of the motor current to describe a time waveform that is post processed as an FFT. Their process is based on

the modulation of the motor current varied (the rotor flux creating counter electromotive force, CEMF) in accordance with a modulating wave. The load variations that repeat are reflected into the stator currents through the motor's CEMF. Demodulate the 60 Hz signal, and what is left is a signature with the load varying frequencies (Bechard, 2001).

Figure 11. PdMA analyzer used in this research (Bethel, 2001).

In a motor operating at 60 Hz, consistently repeating variations in load are reflected back into the stator windings, which causes amplitude changes in current flow with the varying circuit impedance for the changing CEMF. This change is carried through the branch circuit of the motor on the 60 Hz current signal. PdMA is using software-driven amplitude demodulation to remove the 60 Hz signal which is able to

detect motor rotor speed, pole pass, mechanical pass-through and reflected frequencies. A FFT is performed on the demodulated signal resulting in a spectrum that is used in analysis. Without demodulation, the load related frequencies are buried in the noise-to-signal ratio (Bechard, 2001).

Baker Instrument Company

Baker Instrument Company uses motor current signature analysis and instantaneous torque signal. They apply the DFLL to the motor current signal and can calculate very accurate speed with a 10-second sample; they were within 0.008 Hz of actual rotating machinery operating speeds at CPSES. The low resolution FFT does not have the noise-to-signal ratio needed to differentiate low torsional energy.

There are small differences in the methods of data acquisition and analysis, but both the Baker and PdMA systems use Motor Current Signature Analysis. The Baker system also incorporates the torsional portion of the signal as a function of the voltage and current signals transformed to calculate power (Wiedenbrug, 1998).

Figure 12. Baker Instruments Analyzer (Baker Instruments)

Other Projects in Motor Signature Analysis

Georgia Institute of Technology recently published a paper on Motor Current Signature Analysis entitled "A Method for Sensorless On-Line Vibration Monitoring of Induction Motors". This research was a laboratory project based on theoretical analysis, simulated faults, and a linear relationship between the current harmonics and vibration levels. The focus of this research was to evaluate the motor rotor-to-stator displacement against the mechanical vibration signature. After making the correlation, the research was further expanded to determine if sensorless vibration alert levels were possible (Riley, Lin, Haberler, and Schoen, 1997).

Georgia Institute of Technology used current based Motor Electric Signature Analysis that is based on the vibration displacement as a function of the motor current harmonics in the permeance of the rotor to stator system.

> A motor that vibrates from an external source at frequency f_v, will result in an air gap eccentricity that is primarily changing in a fixed axis. This can be modeled as the sum of a forward and backward rotating eccentricity (off center rotation). In many practical applications, the vibration is primarily in the vertical axis, and the winding is at an unknown position. Additional vibration occurs due to rotating asymmetries, such as load unbalance or misalignment. This is modeled as a rotating permeance eccentricity at the rotating frequency.

The permanence variation:

$$P_o(j_s, q_{rm}, w_{r_s}, t) = P_o + \sum_k P_{n,r}\cos[n(j_s - j_{rm}) + a_n]$$
$$+ \sum_k \frac{P_{k,y}}{2}\cos[k(j_s - (b_k - w_{v_k}t))] \qquad (13)$$
$$+ \sum_k \frac{P_{k,y}}{2}\cos[k(j_s - (b_k - w_{v_k}t))]$$

P_o → Average air gap permanence

$P_{n,r}$ → The magnitude of the n-th permanence oscillation at the machine rotating frequency

$P_{k,y}$ → The magnitude of the k-th permanence oscillation at ? $_{v,k}$

? $_{v,k}$ → The frequency of the k-th vibration

a_n and b_k → The phase angles describing the exact position of the stator windings with respect to the vibration.

Permanence Variation Equation Definition (Riley, et.al., 1997)

The results of the experimental model measured the response of a motor upset by an unbalanced disk which was driven by a variable drive motor attached to the same frame. This demonstrated that the motor current sidebands harmonics had a linear response related to the unbalanced disk. This dependence of the current harmonic sum to the frequency of the current demonstrated a need to calculate a proportional constant in sensorless vibration measurement (Riley, et. al., 1997).

From the previous research, the ability to develop a system of vibration severity levels as is found in mechanical vibration models is dependent on the motor air gap permeance and the frequency of the response. The higher the frequency of the vibration

input, the lower the displacement of the rotor, therefore the smaller the resultant current modulation. The smaller the vibration displacement, the smaller the rotor-to-stator flux gap changes due to the reduced displacement the rotor has at higher frequencies. This increases the difficulty in prescribing a precise limit to vibration severity limit due to motor electrical signatures (Riley, et. al., 1997).

A standard relating Motor Electrical Signature Analysis (MESA) for vibration to an absolute value of vibration has not been developed(Riley, Lin, Haberler, and Schoen, 1997). Therefore, the ability to apply know vibration severity limits was not possible in this research. The method of trending the vibration changes and equating them to known physical changes was decided the best method for a proof of concept research. Individual frequencies that are known and used in vibration analysis to determine vibration faults in a motor were chosen as the trending frequencies (Wowk, 1991). Changes in these frequency trends were used to determine if a technology was able to detect the controlled fault mechanism.

CHAPTER 3

METHODS AND MATERIALS

The review of literature in Chapter 2 demonstrates the need to predict the condition of the rotating system in order to avoid incipient failures that could cause excessive equipment downtime and ancillary failures. The review further indicated that, in some fans, the motor electrical signature analysis may not capture all the failure modes. In those cases, other technology could be used to fill the gaps in degradation analysis. This research focused on determining if the use of motor electrical signature analysis and stress wave analysis could detect three types of rotating equipment degradation.

The test subject of this research was a vane-axial fan that was selected as representative of fans in service at Comanche Peak Steam Electric Station (CPSES). The fan was obtained from the CPSES warehouse – a stored spare for a building exhaust fan. The fan was precision balanced prior to staring the test run. One set of bearings was scored on the outer race and the other set of bearings was scored on the inner race. Then the fan was unbalanced with 7.6 grams that resulted in an unbalance of 0.54 ounce inches. All three different conditions were measured using simultaneous data collection of the motor electrical signature, cowling vibration, bearing housing vibration, and stress wave data (the stress wave measurement was part of a parallel project with EPRI).

Research Design

This research used baseline data to compare with the rest of the research data. By designing this research such that all tests were performed in parallel, a comparison in the ability of each technology to successfully detect each artificially induced failure mode was possible. The use of a comparative sampling technique led the results to be reduced using a Paired Comparison Test analysis (Diamond, 1996). This research was designed to control those variables that could be controlled and could affect the motor and fan vibration. Variables that were not expected to affect the results or were uncontrollable (intervening variable) were not controlled.

Controlled Variables

The independent variable or factor which was the focus of this research was the motor rotor response to various deviations from a known optimal operating system. The known optimal system included new bearings, precision balance at each bearing, and a controllable power supply system. A known imbalance of 7.6 grams was attached to jacking bolt at 2 inches from the center of the fan. The imbalance test with good bearings was performed to make a comparison between the controlled sample and the imbalance. After an imbalance comparison run was made, the imbalance was removed and another data set was taken to verify the system was in optimal condition. This test was repeated twice, once with PdMA and again with the Baker Instrument's Motor Electrical Signal Analysis system and SWANTECH's Stress Wave Analysis system (see appendix D).

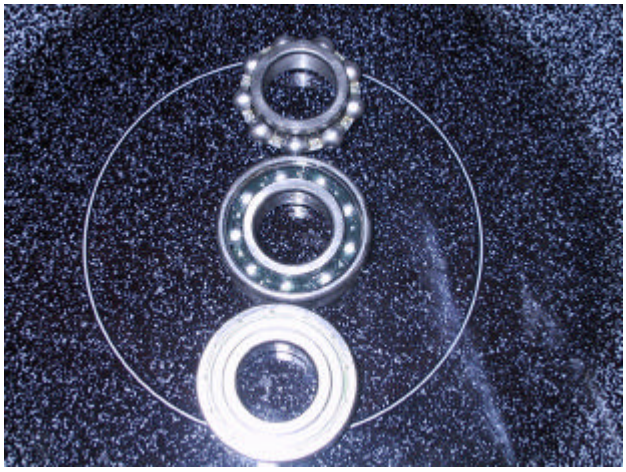

Figure 13. SKF® 6502 deep groove rolling element bearing

The bearing used in the research was a SKF® 6502 deep groove rolling element bearing. Figure 13 shows the complete bearing (bottom), the bearing with the grease shield removed (middle), and the inner race with the balls in the cage (top). The response of motor bearing housings and the cowling response due to changes in the rotating system were other primary factors of interest of this research and were the other independent variables. The mounting of the bearings onto the shaft while minimizing damage was a concern. Damage could introduce another variable into the test. The manufacturer recommends that the bearings be heated in an oil bath or with an induction heater to 250º F to allow the inner diameter of the bearing to fit on the outer diameter of the shaft journal. The bearings are heated because a typical deep grooved rolling element bearing has an interference fit between the inner diameter of the bearing and the outer diameter of the shaft. Overheating the bearing will place the bearing temperature near the annealing temperature of the steel, which will change the hardness of the race and cause plastic deformation under load (SKF 1995).

The installation of the bearings and alignment of the bearings were the moderating variable associated with the dynamic response of the system (Harris, 1988). To control these variables, the same technician using the same equipment installed all the bearings.

Temperature, barometric pressure, and humidity were the moderating variables associated with the test that could affect the fluidic resistance of the air flowing through the fan. This would in turn increase or decrease the load on the motor, affecting the current signature for the motor electrical signal analysis. The test was conducted in an air-conditioned space where the temperature was regulated and verified that barometric pressure and humidity were within 10% of each other for each test (Gastonal, 2001).

We verified the power quality supplied to the motor for each test, the current, voltage, and resistance of the connections could affect the motor current and voltage readings that were used in the analysis. To be valid, the power quality should not differ by more that 1% for the duration of any test (EPRI, 1991).

Uncontrolled Variables

The extraneous variables that were not expected to confuse the results and the intervening variables were not controlled in the research. The controlled variables were measured and if they drifted outside an acceptable level during the data collection, the test was declared invalid.

Sample Size

To determine sample size for this test, an estimate was developed using equation (15), since the variance of the populations was unknown. A valid estimate of the sample size can be computed by:

$d = f(s)$: e.g., with a = 0.05, ß = 0.10, and $d_{diff} = s_{diff}$: (Diamond, 1989) (14)

$d_{diff} = s_{diff}$ → The difference between two means that is important from an engineering viewpoint. In this test case, the important data is the voltage level output of the Digital Signal Processing chip.

f(F)→ Function of the population standard deviant. For the case of Paired Comparison, the $*_{diff}$ is assumed to equal the F_{diff}.

$$N_{pairs} = (U_a + U_b)^2 \frac{s^2_{diff}}{d^2_{diff}} \quad (15)$$

N_{pairs} → Number of trial pairs required or obtained at one level of a variable in the Paired Comparison test.

U_a → Standard normal deviation associated with a type 1 error.

U_b → Standard normal deviation associated with a type 2 error.

The deviations are recovered from a table of deviations for single sided distributions.

Risk and Improvement

In this research, the consequence of committing an Alpha error (a), the alternative hypothesis (H_a) as being true when the null hypothesis (H_o) is actually true, was that it would have claimed: (1) that the cowling vibration was better than the bearing cap data in fault detection. (2) that the motor electrical current signature analysis was able to detect rotor system faults when data did not support fault detection; and (3) the motor electrical torque signature analysis was able detect rotor system faults when data did not support fault detection.

On the other hand, the consequence of committing a Beta error (ß) accepts that the null hypothesis as being true when the alternative hypothesis is actually true, was that it would have claimed: (1) the cowling vibration data was not a better method of fault detection than the bearing cap vibration when it actually was better than bearing cap data. (2) the motor electrical current signature analysis could not detect the difference between baseline data and a faulted rotor system; and (3) the motor electrical torque signature analysis could not detect the difference between baseline data and a faulted rotor system.

The probability of committing an a error is generally chosen to be in the range of 0.01 to .1. In my research, the authors typically used 0.05 when there was no significant difference between a and ß errors (Diamond, 1989; Hinton, 1999; and Sternstein, 1996). For this research, a was chosen to be 0.05. The probability for ß was chosen to be 0.10 due to the variance in vibration data from sample to sample.

In order to determine if the measurement has detected the desired trait, a difference in the population's mean between the baseline and the fault for each condition needed to be tested. The greater the difference between the fault and the baseline data, the smaller the sample size for the same risk. Smaller sample size would reduce the time and cost of the analysis. In addition, there should be a distinct difference between the baseline and faulted rotor system to justify the acceptance of the new technology for use. I could find no comparative data for vane-axial fans for these technologies in my research. Therefore, Paired Comparison was chosen as the approach used to determine if a change was detected for determining the sample size and objective criteria (Diamond 1989).

Sample Size for Research

For this test the following were picked using reference materials (Diamond, W.J. 1989; Hinton, P.R. 1999; Sternstein, M 1996).

$d = f(s)$: e.g., with a = 0.05, ß = 0.10, and $d_{diff} = s_{diff}$:

$$N_{pairs} = (U_a + U_b)^2 \frac{s^2_{diff}}{d^2_{diff}} \qquad (16a)$$

$U_a \rightarrow 1.645$

$U_{ß} \rightarrow 1.282$

$$N_{pairs} = (1.645 + 1.282)^2 \frac{s^2_{diff}}{d^2_{diff}} = 8.6 \qquad (16b)$$

The correct N_{pair} for a *t* distribution:

For sample theory, the number of samples should equal the ? for a *t* distribution by N-1, therefore for this *t* distribution:

? = 8.57 – 1

Nt = 7.57 the U_a and $U_ß$ are determined to be (from lookup tables):

$U_a \rightarrow 1.87$

$U_ß \rightarrow 1.41$

$$N_{pairs} = (1.87 + 1.41)^2 \frac{s^2_{diff}}{d^2_{diff}} = 10.8 \quad (16c)$$

The sample pair size should be eleven (11) samples at random (Diamond, 1989).

Objective Criteria

The methodology for the Paired Comparisons testing after the sample size is determined is to choose at random the sample size from each pair. The difference for each pair is determined and the mean difference and sample variation are calculated (Diamond, 1989):

$$\overline{X}_{diff} = \frac{\sum_{diff} (X_{ia} - X_i)}{11} \quad (17)$$

$$S^2_{diff} = s^2 = \left(\frac{\sum (x_{diff} - \overline{X}_{diff})^2}{n-1}\right) \quad (18)$$

The mean decision criterion is based on the initial population and the standard deviation over the sample size. This gives a “target” for the mean difference to be compared to the original population with a corrected *t* distribution (Diamond, 1989).

$$\overline{X}^{*}_{diff} = m_o + \frac{t_a S_{diff}}{\sqrt{N_{diff}}} \quad (19)$$

The * denotes the criterion mean.

If the difference mean is greater than the criterion, the null hypothesis is accepted for this research with 90 percent confidence (Diamond, 1989).

Test Sequence

The actual test sequence was determined by the time span for each test and the samples taken at specific time within the time span. The numbers of samples ranged from 375 for the vibration to twenty (20) samples for the motor electrical signal analysis data files. Each of the sample times was placed in an Excel spreadsheet and a random number generator was used to select eleven (11) non-rerpetitive samples. The data was then processed for the Paired Comparison test. Table 1 on the following page has a sample of the test data for the motor baseline for bearing casing data. This data was for proof of concept and for validating analysis techniques.

The Trial is the sample file number for the randomly picked imbalance 1X amplitude and Baseline 1X amplitude files. The voltages were either captured directly from the technology used in the comparison, or calculated if the data was in other units to come to a common unit for the comparison.

Trial	Imbalance 1X amplitude (volts)	Baseline 1X amplitude (volts)	Difference in amplitude (volts)
1	0.001401683	0.000835219	0.000566
2	0.001448703	0.000901405	0.000547
3	0.001451159	0.000902928	0.000548
4	0.001451159	0.000923814	0.000527
5	0.001495948	0.000973325	0.000523
6	0.00145034	0.0009259	0.000524
7	0.001402474	0.000925378	0.000477
8	0.001451159	0.000924857	0.000526
9	0.001404057	0.000948282	0.000456
10	0.001451977	0.000947747	0.000504
11	0.001403266	0.000924857	0.000478
		$\sum_{diff}(X_{ia} - X_i)$	0.005678213
		$\overline{X}_{diff}$	0.000525292
		$\overline{X}^{*}_{diff}$	2.83246E-20

Table 1: Imbalance to Baseline, Comparison Model of Vibration on the Bearing Cap.

$(\overline{X}_{diff} = 0.000525292) > (\overline{X}^{*}_{diff} = 2.83246E\text{-}20)$

From Table 1, one conclusion is that the test mean is greater than the mean decision criterion. By the method described by Diamond, this leads the researcher to the conclusion that the Null Hypothesis is rejected and the alternate hypothesis is accepted. This means that with the technology used to compare the imbalance vibration at running speed to the baseline (balanced, new bearings, greased, and inspected), there is a high probability that the measurement identified the change in running speed vibration due to imbalance.

Reject H_o: $\mu_{diff} \neq 0$

Accept H_a: $\mu_{diff} > 0$ with at least 90% confidence. Conclusion: the imbalance amplitude at once per revolution is greater than the baseline 1X amplitude for bearing cap data. This is shown by the comparison of the mean difference being greater than the mean decision criterion.

Test Fan

TXU Comanche Peak Steam Electric Station provided a fan representative of those used in the plant to exhaust air from the Electric Control Buildings. This fan was chosen because the internal support system has a long transmission path between the motor bearings and the external fan cowling (can), and the limited power available to run the fan in the test area. In addition, this type of fan is used to supply and exhaust air in many applications within the Electrical Utilities (EPRI, 1991). The fan provided was a 24 inch vane axial fan manufactured by Aerovent using a direct drive from a Baldor motor: 5 Hp motor, 3 phase, 460 VAC, 6.4 Amps (full load), 1778 RPM motor. Figure 14 depicts the fan utilized in this research.

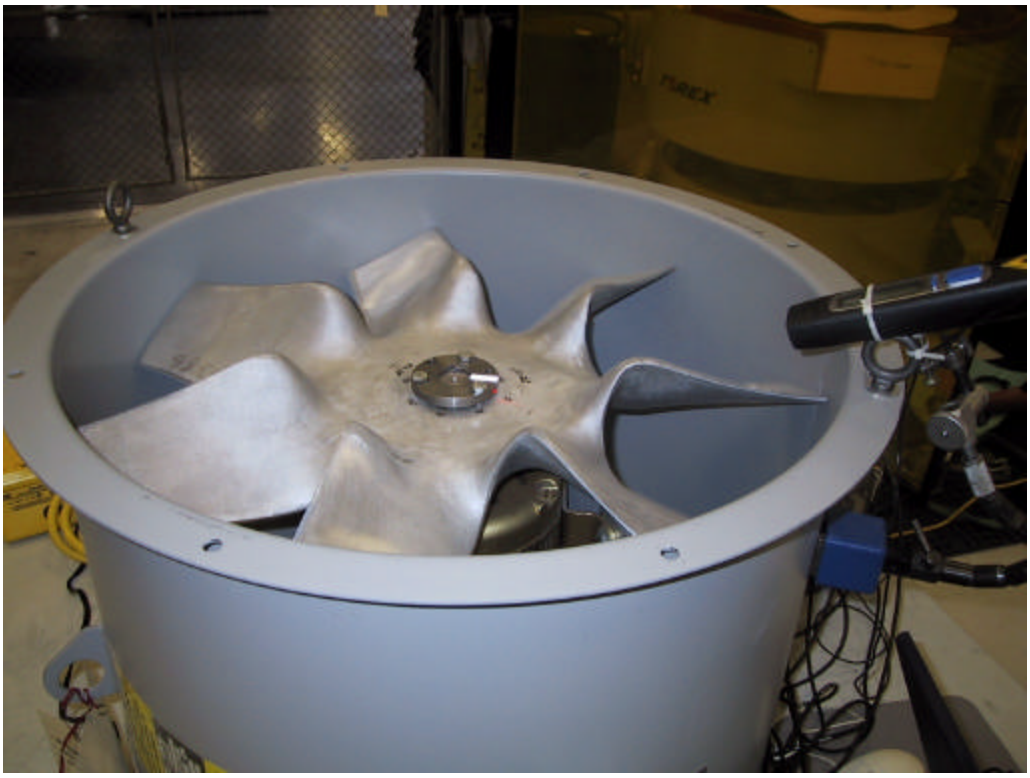

Figure 14. Aerovent 24-inch vane-axial fan.

As can be seen in Figure 14, the fan has seven (7) blades. The air is drawn over the fan blades, down around the motor, and out into the ventilation ductwork. For this test the fan was mounted on a frame with a very low natural frequency (shown in figure 15), less than 1/10 of the running speed of the motor. The low natural frequency was chosen to ensure that the test frame would not interfere with the test data (Harris, 1988).

In Figure 15, the fan is shown attached to the test base in the Maintenance shop at CPSES. A Bently Nevada multi-channel analyzer is on the left, and on the right is the backup tape recorder with a 12 channel PCB power supply for the accelerometers on top. All signals from the vibration probes were parallel between the Bently Nevada system and the digital tape recorder.

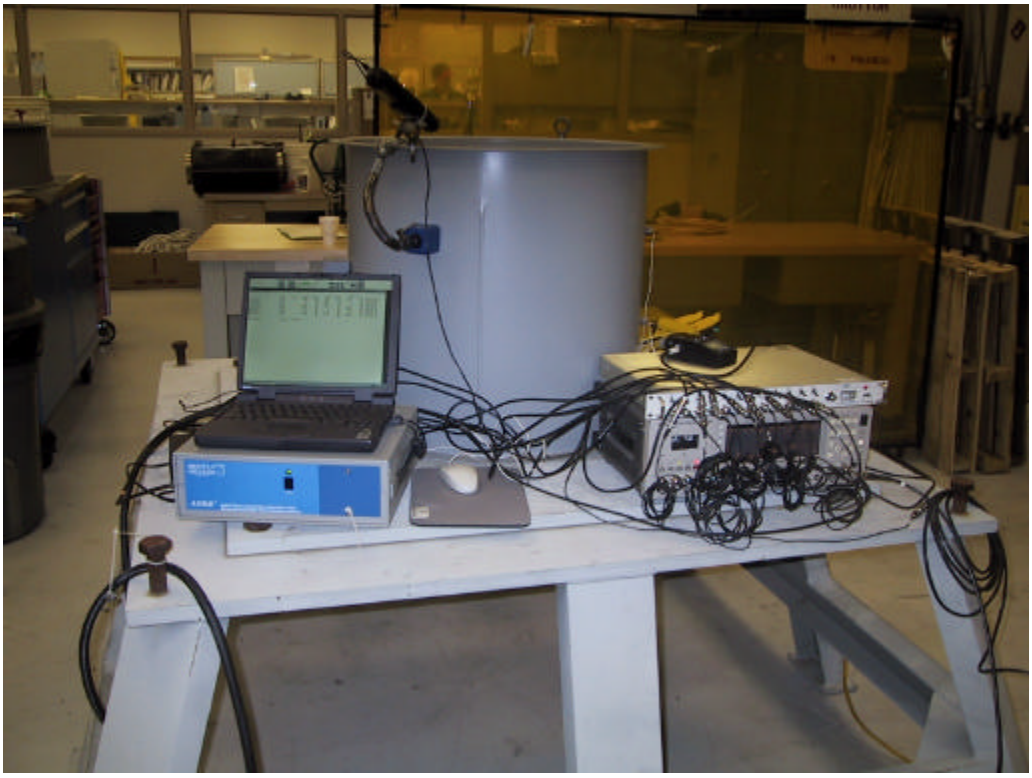

Figure 15. Fan mounted on test frame.

The fan is attached to the motor with a conical hub. Three (3) bolts secure the fan to the motor shaft as can be seen in Figure 16. The conical hub is keyed to prevent the fan from slipping during starting and running operations. In “front” of the fan is a diffuser plate used to provide less turbulent air to the fan blades. The diffuser “straightens” the air and helps maintain even load distribution on the fan blades. The diffuser was not attached to the fan during the testing, to allow access to the fan for balancing and bearing replacements. The laser tachometer was used for speed verification for the Bently Nevada system and to compare to the Motor Electrical Signature Analysis systems speed references.

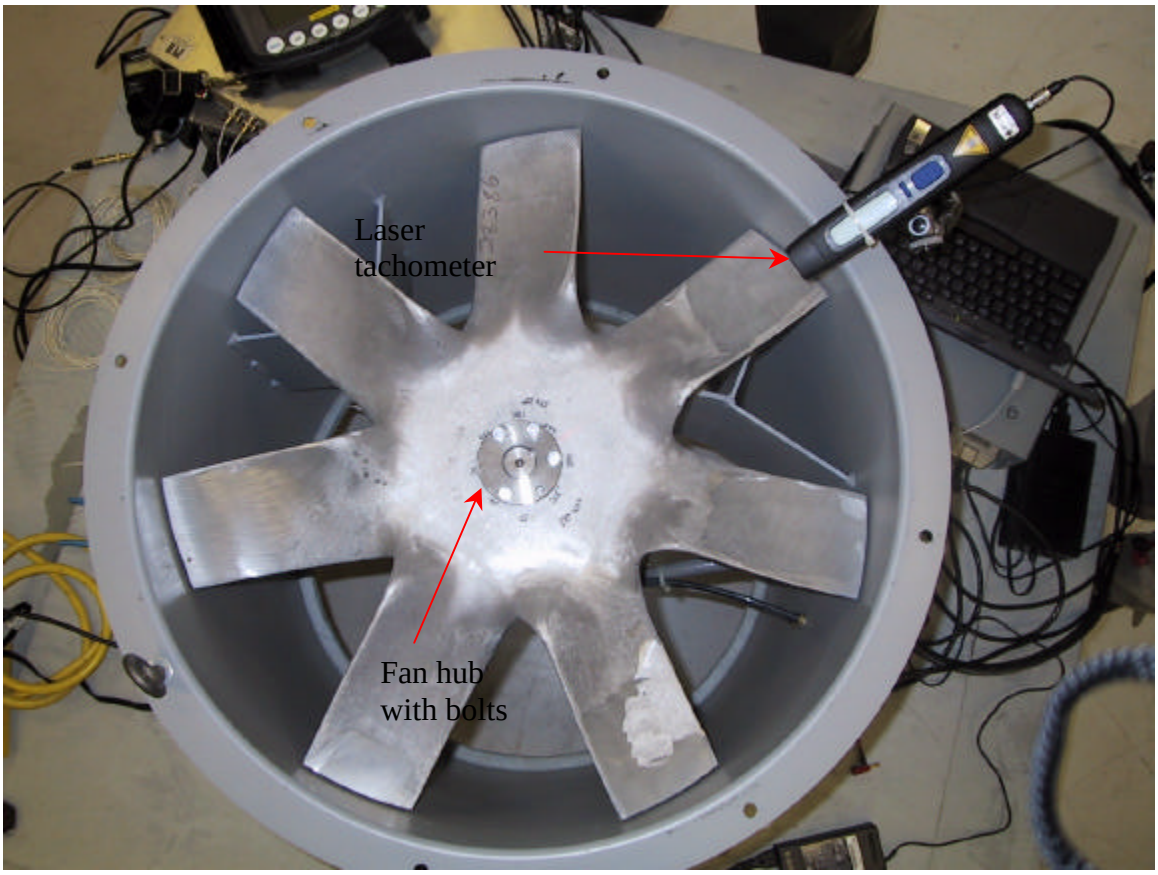

Figure 16. Fan hub.

Three different analysis techniques were used during this research and five different instruments were employed. The first two were vibration systems: the Cognitive Systems CV395B spectrum analyzer, the Bently Nevada, ADRE 208P vibration data acquisition system (ADRE - Automated Diagnostics for Rotating Equipment), and the SWANTECH stress wave analysis system (EPRI project).

Figure 17 shows the Cognitive System along with specifications listed in table 2. The Cognitive Visions CV395B is a 4 channel real time analyzer, with multiple functions built in for traditional vibration data analysis including: transfer functions, FFT spectrums, time waveforms, 1/3rd octave sound analysis, and balancing.

Figure 17. Cognitive Vision CV395B.

	Cognitive Vision CV395B
Frequency Range	DC to 100 kHz
A/D	16 bit
Dynamic Range	90 dB
FFT Resolution	100 – 2400 lines
Input impedance	1 MO +1.5%
Power	AC power

Table 2. CV395B specifications

Figure 18 depicts the ADRE system along with its specifications in Table 3. The ADRE 208P system is an eight channel dynamic analyzer. It was originally developed for capturing planned transients on large journal bearing machines. With new advances, the system can measure many different types of transducers and collect all eight channels in a very short period of time. The system is optimized for data collection of transient systems and steady state operations, which were the focus of this research.

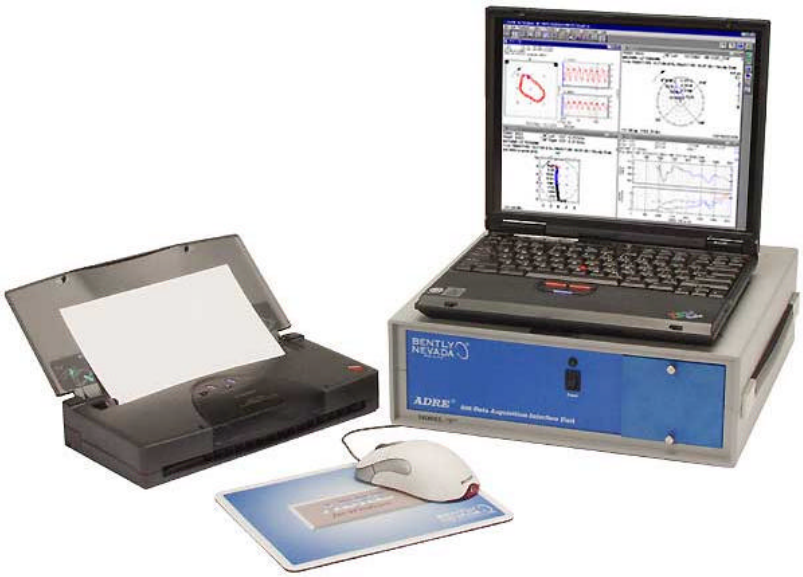

Figure 18. Bently Nevada ADRE.

	Bently Nevada ADRE 208-P
Frequency Range	DC to 10kHz
A/D	12 bit
Dynamic Range	66 dB
FFT Resolution	100 – 1200 lines
Input impedance	1 MO $\pm$3%
Battery power	4 hr NiCa Battery

Table 3. Bently Nevada Specifications

The CV395B was used to analyze the data saved to the digital tape in order to verify the transient and steady state vibration data collected with the ADRE 208P system. The ADRE data was backed up in parallel to a digital tape recorder a TEAC RD-120 16-

channel tape system, shown in Figure 19. Once the ADRE data was reviewed and verified, the TEAC tapes were stored for future testing and analysis.

Figure 19. Vibration data acquisition station.

In Figure 19, the data acquisition setup for the Baker and SWANTECH testing is displayed. The tape was in parallel to the ADRE 208P system, and under the TEAC digital tape deck is the 12 channel PCB, ICP accelerometer power supply.

The other test equipment used for vibration data collection were the vibration accelerometers, laser tachometer, thermocouples, air flow meter, current meter, multi-meter, and humidity meter. The vibration detectors were all 100 mV/g ICP transducers, which were installed on the bearing housings and the fan cowling as seen in Figures 21 and 22.

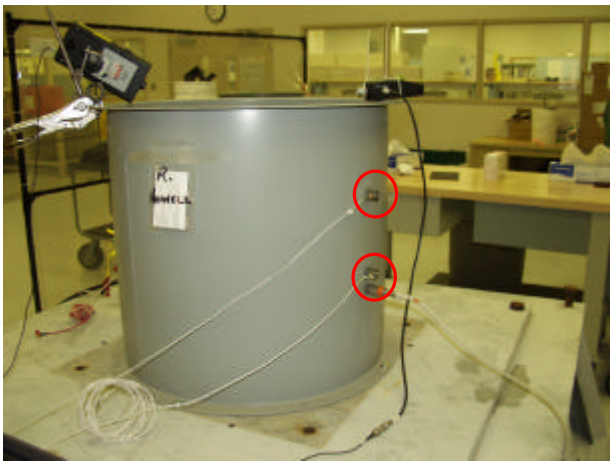

Figure 20. Fan cowling vibration transducers.

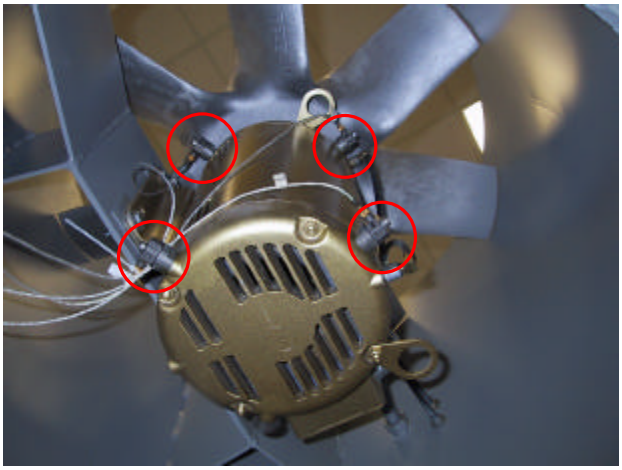

Figure 21. Motor bearing housing transducers.

In Figures 20 and 21, the locations of the vibration transducers are circled. The vibration transducers were attached with studs to washers that were affixed to the fan and cowling with epoxy. Figure 20 show the two tri-axial vibration transducers attached to the fan cowling and Figure 21 depicts the location of the four tri-axial vibration transducers attached to the fan motor bearing housings. The natural frequency of the washers and transducers was > 5 kHz. The transducers were connected to a 12 channel

power supply that amplified the vibration signal and sent it to the ADRE system and TEAC digital tape recorder.

There were two different motor electrical signal analysis systems as part of this research. The first was the PdMA EMax (Figure 22).

Figure 22. PdMA EMax portable dynamic tester.

	Emax
Frequency Range	100 kHz
A/D	16 bit
Dynamic Range	138 dB *
FFT Resolution	100 – 12,800 lines
Input impedance	1 MO ±3%
Power	AC power

Table 4. Emax specifications. *The Emax dynamic range is improved through gain amplification of the 16 bit signal.

The Emax system from PdMA Corporation, is a portable dynamic tester that evaluates electrical motor condition without shutting down process (Figure 23). The system was originally designed specifically for motor electric circuit analysis. With the addition of demodulated motor current analysis, the system now measures mechanical as well as electrical motor system problems. Table 4 lists the specifications for the system. One item of interest is the 138 dB gain possible with the system – the 16 bit digital system has ~ 90 dB dynamic range, with gain after demodulation 138 dB is possible.

Current is collected in one of three ways: high resolution, low resolution or eccentricity. Each uses different sampling rates and resolutions to identify anomalies in a specific fault zone. Rotor bar defects and eccentricity, static or dynamic are detected and trended. Graphing in-rush current and startup time is extremely valuable when evaluating motor operation and condition. Changes in the startup characteristics can be attributed to rotor or stator faults. Figure 23 shows the FFT (spectrum) of eccentricity measurement made by the PdMA EMax system from the demodulated current signal. This is a FFT spectrum with frequency on the X axis and amplitude of the data in dB current on the Y axis.

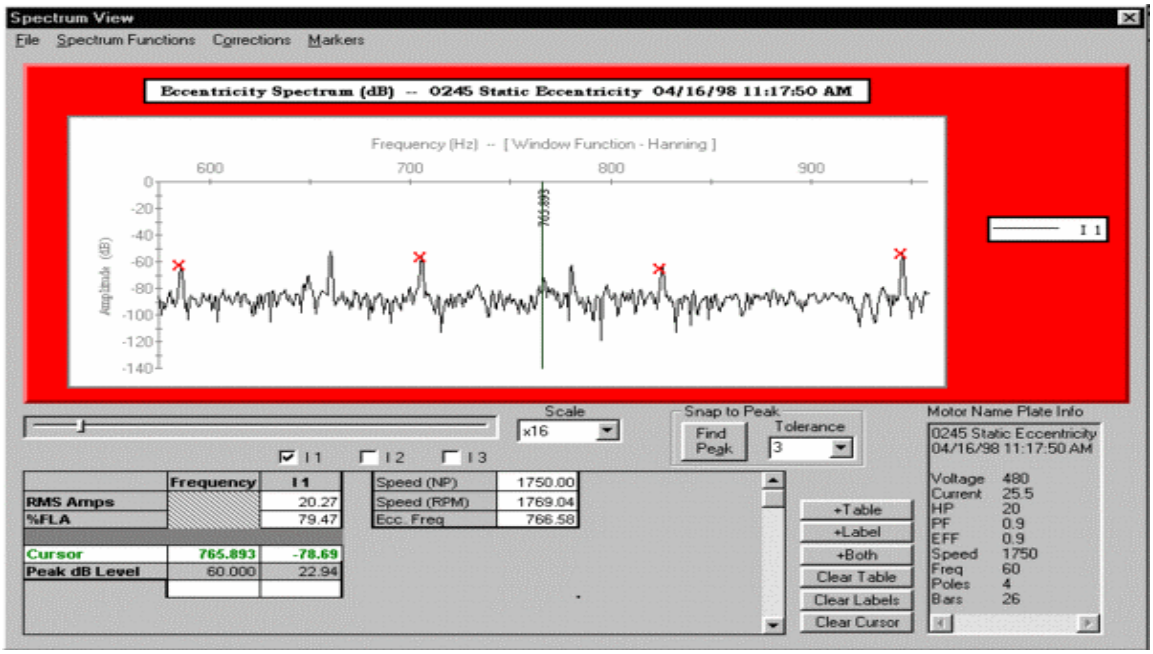

Figure 23. PdMA Emax spectrum screen print.

Emax reports include a series of graphs, screen plots and historical comparisons. In addition, the Emax next generation of software used the Motor Current Spectrum in testing at CPSES to monitor for motor rotor mechanical dynamics such as motor speed, imbalance, bearing faults, vane pass, and other mechanical rotating parameters.

The second system was the MPM Explorer which is shown in Figure 24. The Baker Instrument MPM system specifications are listed in table 5. The MPM system uses a 12 bit analog-to-digital converter with gain and noise reduction circuitry and has a dynamic range of 138 dB (a 12 bit analog to digital system typically has approximately 66 dB resolution).

Figure 24. Baker Instruments MPM portable dynamic tester.

	MPM
Frequency Range	100 kHz
A/D	12 bit
Dynamic Range	138 dB
FFT Resolution	100 – 1,200 lines
Input impedance	1 MO ±3%
Power	AC power

Table 5. MPM specifications

This self-contained portable instrument is computer driven and all testing can be accomplished directly from the Motor Control Center. The Performance Monitor (Motor Performance Monitor - MPM) Explorer Series II performs five major functions in a complete predictive maintenance program. (1) It identifies possible power circuit problems that degrade motor health; (2) examines overall motor power conditions; (3) monitors the load; (4) observes motor performance; and (5) estimates energy savings. It also can analyze the instantaneous torque with a FFT spectrum or DFLL wavelet system.

For this research the FFT spectrum was utilized. The DFLL module was not completely developed in time for this testing.

The MPM is programmed to supply information on voltage balance, distortion, voltage level, rotor cage condition, motor efficiency, effective service factor, and over current, along with torque ripple and load history. This wide range of tests allows the exploration of the true condition of motor integrity and the conditions related to motor performance.

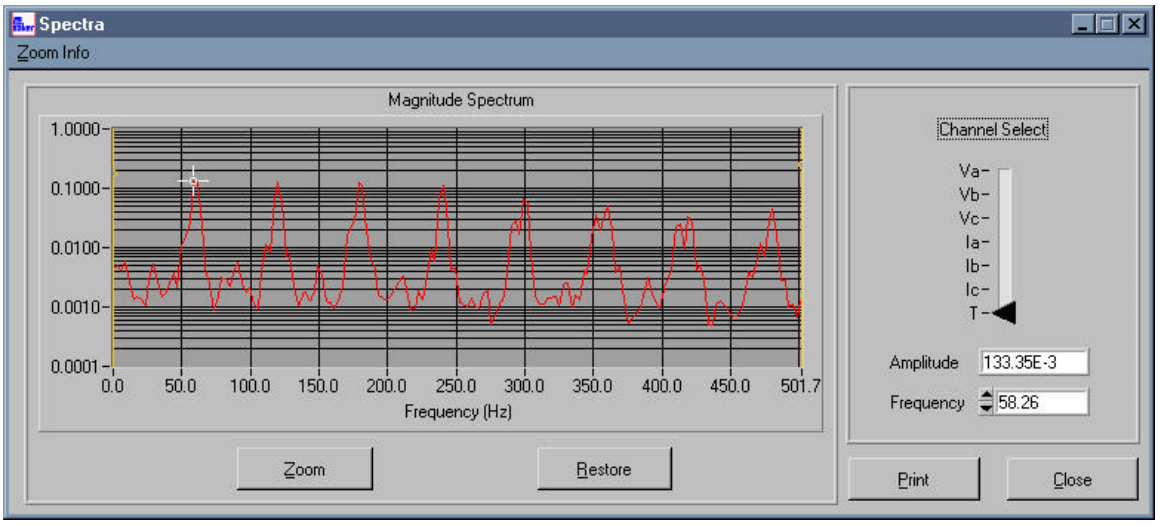

Figure 25. Baker MPM spectrum screen print.

For any test, the spectra data from voltage, current, or torque is available. Figure 25 is a screen print of torque spectrum taken from the baseline test for the EPRI project. The torque data is demodulated because the torque is a function of the rotor speed. The torque spectra were used for the different tests at Comanche Peak.

Another vibration technology was reviewed for EPRI during this research. The technology is called Stress Wave Analysis. It uses an accelerometer with a natural mounted frequency of 40 kHz. This accelerometer is connected to an analog band-pass

filter that filters frequencies below and above 40 kHz. The output is rectified and fed into an analog-to-digital circuit. The system is shown in Figure 27 during the EPRI testing of the fan system.

Figure 26. SWANTECH data collection system.

The system shown in Figure 26 is a SWANview® portable analyzer. It collects data from two field transducers, which are tuned accelerometers designed to have a resonance frequency of ~ 40 KHz. The transducer's outputs are analog filtered at the computer with a band pass filter around 40 KHz. This frequency limits mechanical information due to the fundamental frequencies (mechanical noise) from entering the process. The data is then processed by digital filters and demodulated to go into the analyzer which is designed to measure the stresses in the system, along with a FFT spectrum and a histogram of the Gaussian curve for the demodulated data.

This data was used to verify the ability of stress wave analysis to detect rolling element bearing faults with sensors connected to the cowling of the suspect motor. This

data was used to verify the bearing cap data taken with normal accelerometers and spectrum analysis.

Sample Preparation

The test group of bearings was staged and two bearings were picked, at random, to be modified for the test. Two bearings were artificially flawed. One had the outer race scored (Figure 27) and one bearing had the inner race scored (Figure 28) with an abrasive high-speed grinder. These bearings were for the conceptual test of detecting bearing faults using motor electrical signature analysis. The rest of the bearings were used for baseline data collection and returning the motor and fan to the condition found on receipt.

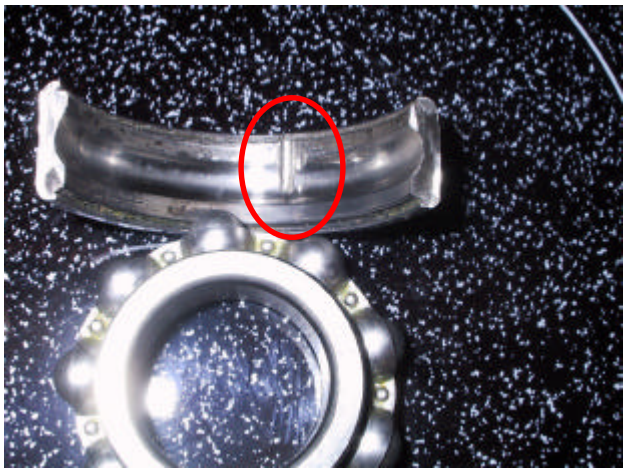

Figure 27. SKF® 6503 deep groove bearing.

The outer race defect in Figure 27 was taken after the testing was complete. The bearing outer race was cut into two pieces and the bearing analyzed. The groove in the outer race was ½ inch long, 1/16 inch wide, and 1/16 inch deep. This would be considered a failure type flaw in a rolling element bearing (Berry, 1994).

Figure 28. SKF® 6502 deep grooved bearing.

The inner race defect in Figure 28 was taken after the testing was complete. The bearing outer race was cut into two pieces and the bearing analyzed. The groove in the outer race was 2/3 inch long, 1/16 inch wide, and 1/16 inch deep. This would be considered a failure type flaw in a rolling element bearing (Berry, 1994).

Test Procedure

The fan tests were run in two separate groups: one with PdMA and the other with Baker and SWANTECH. Each group test consisted of a baseline run, an imbalanced fan run, a faulted bearing run, and a baseline verification run. Prior to running the first test with PdMA, new bearings were installed in the fan and the fan was balanced. Once the vibration data from the bearing housing was analyzed for any bearing faults or imbalance, the first baseline data was collected using ADRE, the TEAC digital tape recorder, and the PdMA Emax system. This same sequence was followed for the Baker MPM and SWANTECH SWANview® testing a week later.

After the baseline run, a weight was attached 2 inches from the centerline of the shaft on the fan-coupling hub as shown in Figure 30. This introduced an eccentric imbalance on the fan end of the motor, which translates 0.54 oz-inch of additional imbalance (see equation 20) in the motor bearing housings. This equated to a doubling of the vibration in inches per second at the motor outboard bearing. The motor was started and the first set of comparison data was collected.

$$\begin{aligned} &\text{Imbalance } = r\,(radius) * \ mass \\ &imbalance\,(oz-inch) = r*m-grams\,(\frac{0.03527oz}{1\,gram}) \\ &imbalance = 2\,inches*\frac{7.6\,grams*0.03527\,oz}{gram} \\ &imbalance = 0.54\ oz-inch \end{aligned} \tag{20}$$

Figure 29 shows the fan hub with the imbalance weights attached in the top of the bolt ring. The weights between the bolts on the right side of the picture were the weights added to balance the fan prior the test baseline run. These weights were not removed for the remainder of the testing.

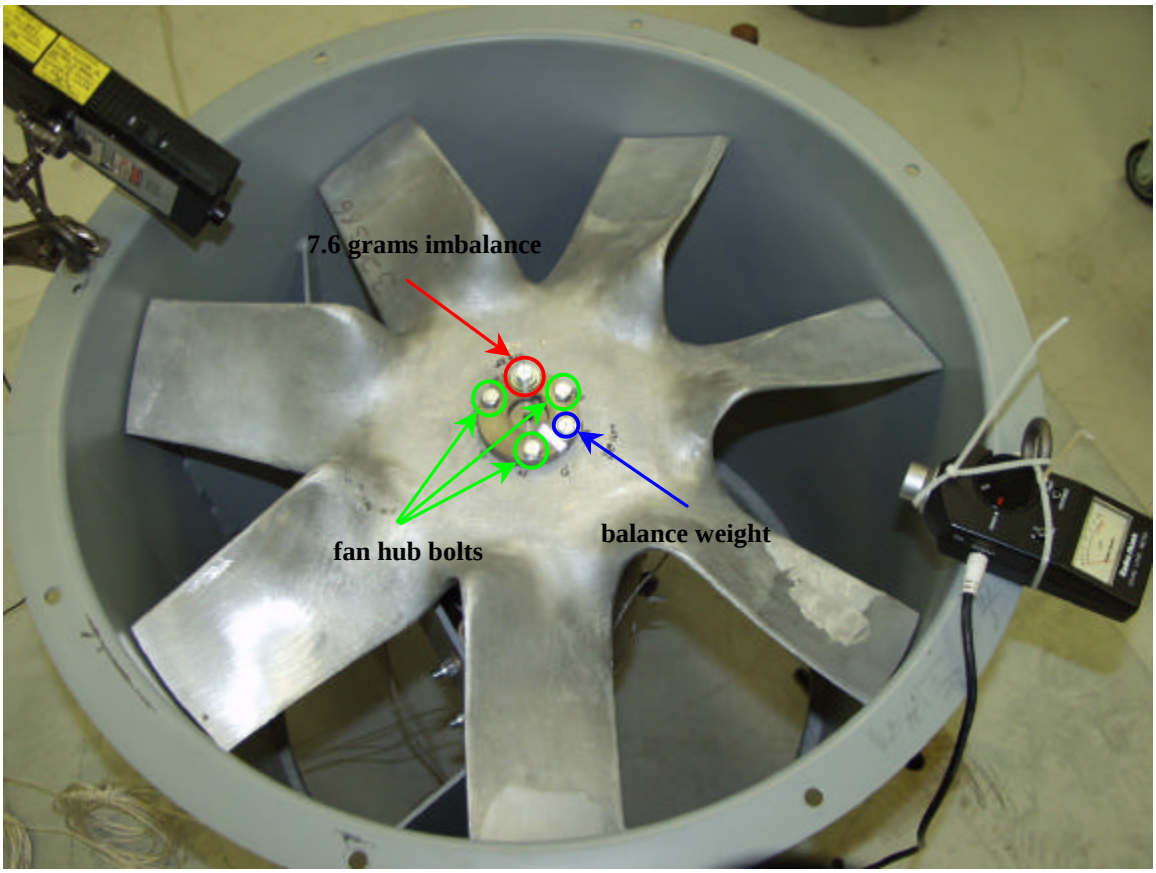

Figure 29. Fan with imbalance weight.

After the imbalance run, the outboard (free end) bearing was removed and a faulted inner race bearing was installed. The bearing removal of the bearing is shown in Figures 30 and 31. Figure 30 shows the bearing puller being used on the motor outboard bearing, with the motor still attached to the fan (inboard side). A new bearing could not be re-used if it was removed by this method.

Figure 31 is a picture of the motor outboard bearing housing, removed from the motor to gain access to the bearing on the motor shaft. The bearings have to be heated to install because there is about 0.002 inches difference between the bearing inner diameter and the shaft outer diameter.

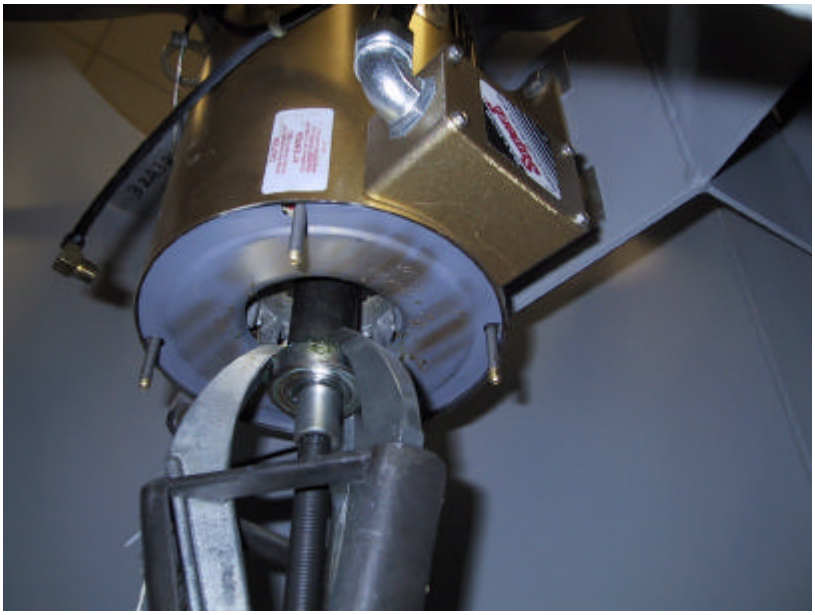

Figure 30. Removal of bearing from motor outboard end.

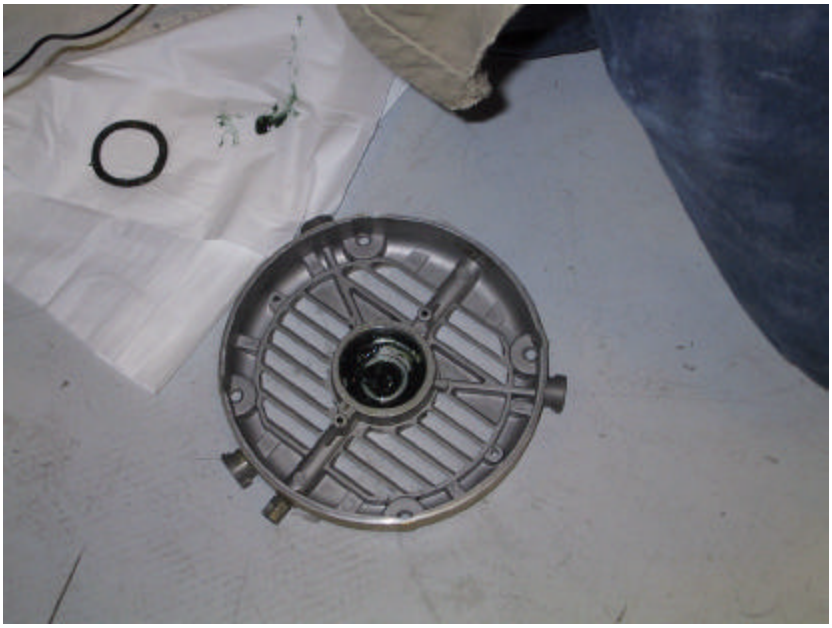

Figure 31. Motor outboard bearing housing (end bell).

The motor was reassembled, balance was checked, the motor continued to run for five minutes, then motor data was collected along a with ADRE and TEAC digital tape recording of the bearing housing and fan cowling vibration data.

The test data was collected simultaneously for all tests to reduce any errors due to changes in running condition. The motor current, voltage, temperature, running speed, vibration, noise level, humidity, and air temperature were collected to identify any conditions that would invalidate the test. During the Baker / SWANTECH data collection, the load and air borne noise were lower than during the PdMA testing. The fan was found to be running backwards. This invalidated the first three runs of the Baker test, which had to be performed over.

Figure 32. Collecting data during the PdMA testing.

In Figure 32, data collection for the first baseline data collection run is in progress with the PdMA test equipment. Notice that the data collection system is near the power supply console. The fan is about 25 feet to the left of the picture. The data collection systems were close to the power supply to simulate conditions found in our power plant, where the Motor Control Cabinets are remote in relationship to the fans.

CHAPTER 4

RESULTS AND ANALYSIS

Fan motor testing was conducted at the TXU SMART Team Three equipment repair and inspection shop. The area was used exclusively for this research. The results were downloaded off the different databases and transferred to Microsoft® Excel spreadsheets. Test of the objective criterion, using the equations discussed in chapter 3, was the primary method employed to analyze the test data. The vibration data on the fan cowling did have measurable changes in amplitude at the specific frequencies of concern for this comparison test, but the levels, once translated to vibration velocity (inches per second), were in the noise floor of the overall signal. Additionally, the Stress Wave Analysis data was used in validation of this new technology for future investigations.

Tests of Objective Criteria

Tables 6, 7, 8, 9, 10, 11, and 12 are based on the Comparative Analysis and show the results of the testing compared to the objective criteria. Each of these tables contains the average standard variance, test criterion, and the difference in means between the baseline and the test conditions for each test.

Tables 5, 6, and 7 correspond to research question #1: Will the use of cowling mechanical vibration detect faults in the motor rotor system compared to the bearing housing mechanical vibration? The objective criteria were computed using equation (19). Table 10 shows that the cowling data rejects the null hypothesis, and therefore can differentiate between baseline and motor imbalance conditions. Tables 6 and 7 indicate

that the cowling data accepts the null hypothesis and therefore cannot differentiate between baseline data and motor bearing faults.

Fan cowling imbalance data with statistical calculations is shown in table 6. This table is a comparison between the Baseline running speed vibration taken on the cowling and the imbalance running speed vibration taken on the cowling. Running speed vibration is the frequency data that is used to determine imbalance.

Trial	Imbalance 1X amplitude (volts)	Baseline 1X amplitude (volts)	Difference in amplitude (volts)
1	0.0003065	0.0002872	1.93193E-05
2	0.0003065	0.000287	1.94814E-05
3	0.0003063	0.0002872	1.91464E-05
4	0.0003063	0.0002872	1.91464E-05
5	0.0003063	0.000287	1.93085E-05
6	0.0003062	0.000287	1.91356E-05
7	0.000306	0.0002872	1.88006E-05
8	0.0003062	0.0002872	1.89735E-05
9	0.0002633	0.0002874	-2.40951E-05
10	0.0003062	0.0002872	1.89735E-05
11	0.0003063	0.0002874	1.89843E-05
		$\sum_{diff}(X_{ia} - X_i)$	3.787E-06
		$\overline{X}_{diff}$	1.51977E-05
		$\overline{X}^*_{diff}$	8.85145E-22

Table 6: Imbalance to Baseline, Comparison Baseline to imbalanced measured on the cowling with accelerometers.

($\overline{X}_{diff}$ = 1.51977E-05) > ($\overline{X}^*_{diff}$ = 8.85145E-22)

Reject H_o: $\mu_{diff} \leq 0$

Accept H_a: $\mu_{diff} > 0$ with at least 90% confidence. Conclusion: the imbalance which is indicated by the once per revolution amplitude is greater than the baseline once per revolution amplitude for fan cowling data.

Fan cowling bearing inner race (Ball Pass Inner Race, BPIR) fault data with statistical calculations is shown in table 7. This table is the comparison between the Baseline BPIR vibration taken on the cowling and the faulted inner race BPIR data taken on the cowling. BPIR vibration is the frequency data that is used to determine bearing inner race defects.

Trial	BPIR amplitude (volts)	BPIR baseline amplitude (volts)	Difference in amplitude (volts)
1	0.0000259	0.0002593	-0.000233387
2	0.0000259	0.0002593	-0.000233387
3	0.0000259	0.0001297	-0.000103728
4	0.0000259	0.0001297	-0.000103728
5	0.0000259	0.0002593	-0.000233387
6	0.0000259	0.0002593	-0.000233387
7	0.0000259	0.0002593	-0.000233387
8	0.0000259	0.0002593	-0.000233387
9	0.0000259	0.0001297	-0.000103728
10	0.0000259	0.0001297	-0.000103728
11	0.0000259	0.0001297	-0.000103728
		$\sum_{diff}(X_{ia} - X_i)$	-0.001918963
		$\overline{X}_{diff}$	-0.000174451
		$\overline{X}^*_{diff}$	0

Table 7: BPIR to Baseline, Comparison Baseline to an inner race defect measured on the cowling with accelerometers

$(\overline{X}_{diff} = -0.000174451) < (\overline{X}^*_{diff} = 0)$

Accept H_o: $\mu_{diff} \leq 0$ with at least 90% confidence.

Reject H_a: $\mu_{diff} > 0$

Conclusion: Accept Null Hypothesis that the BPIR amplitude is less than the baseline amplitude for fan cowling data. Fan cowling data is inconclusive in detection of BPIR faults.

Fan cowling bearing outer race (Ball Pass Outer Race BPOR) fault data with statistical calculations is shown in table 8. This table is the comparison between the Baseline BPOR vibration taken on the cowling and the faulted outer race BPOR data taken on the cowling. BPOR vibration is the frequency data that is used to determine bearing outer race defects.

Trial	BPOR amplitude (volts)	BPOR baseline amplitude (volts)	Difference in amplitude (volts)
1	2.593E-05	8.59E-05	-5.99676E-05
2	2.593E-05	8.59E-05	-5.99676E-05
3	2.593E-05	8.59E-05	-5.99676E-05
4	2.593E-05	8.59E-05	-5.99676E-05
5	2.593E-05	1.718E-05	8.75203E-06
6	2.593E-05	8.59E-05	-5.99676E-05
7	2.593E-05	8.59E-05	-5.99676E-05
8	2.593E-05	8.59E-05	-5.99676E-05
9	2.593E-05	8.59E-05	-5.99676E-05
10	2.593E-05	8.59E-05	-5.99676E-05
11	2.593E-05	8.59E-05	-5.99676E-05
		$\sum_{diff}(X_{ia} - X_i)$	-0.000590924
		$\overline{X}_{diff}$	-5.37203E-05
		$\overline{X}^{*}_{diff}$	1.77029E-21

Table 8: BPOR to Baseline, Comparison Baseline to an outer race defect measured on the cowling with accelerometers

($\overline{X}_{diff}$ = -5.37203E-05) < ($\overline{X}^{*}_{diff}$ = .77029E-21)

Accept H_o: $\mu_{diff} \leq 0$ with at least 90% confidence.

Reject H_a: $\mu_{diff} > 0$

Conclusion: Accept Null Hypothesis that the BPOR amplitude is less than the baseline amplitude for fan cowling data. Fan cowling data is inconclusive in detection of BPOR faults.

Tables 8, 9, 10, and 11 correspond to research question #2 which is divided into two parts due to the differences in the methodology of data analysis performed by Baker and by PdMA. The motor electrical signature analysis failed to accept the null hypothesis and therefore accepted the alternate hypothesis; motor current analysis can detect motor faulted conditions.

PdMA imbalance data with statistical calculations is shown in table 9. This table is a comparison between the baseline running speed vibration taken with the PdMA motor current analyzer and the imbalance running speed vibration taken with the PdMA box. The running speed vibration is the frequency data that is used to determine imbalance.

Trial	Imbalance 1X amplitude (volts)	Baseline 1X amplitude (volts)	Difference in amplitude (volts)
1	0.775692	0.547031	0.22866091
2	0.765692	0.537031	0.22866091
3	0.745692	0.587031	0.15866091
4	0.695692	0.497031	0.19866091
5	0.665692	0.541203	0.12448871
6	0.725692	0.547031	0.17866091
7	0.595692	0.557031	0.03866091
8	0.769692	0.549931	0.21976091
9	0.761692	0.547031	0.21466091
10	0.742692	0.511231	0.23146091
11	0.775692	0.546131	0.22956091
		$\sum_{diff}(X_{ia} - X_i)$	2.0518978
		$\overline{X}_{diff}$	0.18653616
		$\overline{X}^{*}_{diff}$	3.98811E-17

Table 9: Imbalance to Baseline, Comparison using PdMA Emax system

($\overline{X}_{diff}$ = 0.18653616) > ($\overline{X}^{*}_{diff}$ =3.98811E-17)

Table 9 analysis continued:

Reject H_o: $\mu_{diff} \neq 0$

Accept H_a: $\mu_{diff} > 0$ with at least 90% confidence. Conclusion: the imbalance which is indicated by the once per revolution amplitude is greater than the baseline once per revolution amplitude for the PdMA motor electrical signature analysis data.

PdMA bearing inner race (Ball Pass Inner Race BPIR) fault data with statistical calculations is shown below in table 10. This table is a comparison between the Baseline BPIR vibration taken with the PdMA Emax system and the faulted outer race BPIR data taken with the PdMA Emax system. BPIR vibration is the frequency data that is used to determine bearing inner race defects.

Trial	BPIR amplitude (volts)	BPIR Baseline amplitude (volts)	Difference in amplitude (volts)
1	0.14632136	0.12555643	0.02076493
2	0.14487030	0.11235864	0.032511657
3	0.14511590	0.11153624	0.033579657
4	0.14511590	0.13568943	0.009426473
5	0.14959480	0.10120643	0.048388373
6	0.14503400	0.13565664	0.009377357
7	0.14024740	0.10125343	0.038993973
8	0.14511590	0.13589627	0.009219625
9	0.14040570	0.11478275	0.025622951
10	0.15519770	0.12756427	0.027633425
11	0.14032660	0.11996843	0.020358173
		$\sum_{diff}(X_{ia} - X_i)$	0.275876592
		$\overline{X}_{diff}$	0.02507969
		$\overline{X}^*_{diff}$	2.71917E-18

Table 10: BPIR to Baseline, Comparison of Baseline and bearing inner race defect using the PdMA Emax system

($\overline{X}_{diff}$ = 0.02507969) > ($\overline{X}^*_{diff}$ = 2.71917E-18)

Table 10 continued:

Reject H_o: $\mu_{diff} \neq 0$

Accept H_a: $\mu_{diff} > 0$ with at least 90% confidence. Conclusion: the BPIR amplitude is greater than the BPIR baseline amplitude for PdMA motor electrical signature analysis data.

Baker imbalance with statistical calculations is shown below in table 11. This table is a comparison between the baseline running speed vibration taken with the Baker motor analyzer and the imbalance running speed vibration taken with the Baker box. The running speed vibration is the frequency data that is used to determine imbalance.

Trial	Imbalance 1X amplitude (volts)	Baseline 1X amplitude (volts)	Difference in amplitude (volts)
1	0.019950	0.0001334	0.0198166
2	0.019950	0.0001334	0.0198166
3	0.019110	0.0001334	0.0189766
4	0.021130	0.0001334	0.0209966
5	0.021130	0.0001334	0.0209966
6	0.019950	0.0001413	0.0198087
7	0.019950	0.0001334	0.0198166
8	0.019950	0.0001259	0.0198241
9	0.020540	0.0001413	0.0203987
10	0.019950	0.0001413	0.0198087
11	0.021130	0.0001334	0.0209966
		$\sum_{diff}(X_{ia} - X_i)$	0.2212564
		$\overline{X}_{diff}$	0.020114218
		$\overline{X}^*_{diff}$	4.53194E-19

Table 11: Imbalance to Baseline, Comparison using Baker MPM system

($\overline{X}_{diff}$ = 0.020114218) > ($\overline{X}^*_{diff}$ =4.53194E-19)

Reject H_o: $\mu_{diff} \neq 0$

Table 11 continued:

Accept H_a: $\mu_{diff} > 0$ with at least 90% confidence. Conclusion: the imbalance which is indicated by the once per revolution amplitude is greater than the baseline once per revolution amplitude for Baker MPM motor electrical signature analysis data.

Baker MPM bearing outer race (Ball Pass Outer Race BPOR) fault data with statistical calculations is shown in table 1.2 This table is a comparison between the Baseline BPOR vibration taken with the Baker MPM system and the faulted outer race BPOR data taken with the Baker MPM system. BPOR vibration is the frequency data that is used to determine bearing outer race defects.

Trial	BPOR amplitude (volts)	BPOR Baseline amplitude (volts)	Difference in amplitude (volts)
1	0.01778	0.01334	0.00444
2	0.01679	0.01585	0.00094
3	0.01778	0.01655	0.00123
4	0.01911	0.01585	0.00326
5	0.01778	0.01778	0
6	0.01778	0.01585	0.00193
7	0.01911	0.01679	0.00232
8	0.01679	0.01585	0.00094
9	0.01334	0.01778	-0.00444
10	0.01778	0.01778	0
11	0.01778	0.01585	0.00193
		$\sum_{diff}(X_{ia} - X_i)$	0.01255
		$\overline{X}_{diff}$	0.001140909
		$\overline{X}^{*}_{diff}$	2.83246E-19

Table 12: BPOR to Baseline, Comparison of Baseline and bearing inner race defect using the Baker MPM system

($\overline{X}_{diff}$ = 0.001140909) > ($\overline{X}^{*}_{diff}$ = 2.83246E-19)

Reject H_o: $\mu_{diff} \neq 0$

Table 12 continued:

Accept H_a: $\mu_{diff} > 0$ with at least 90% confidence. Conclusion: the BPOR amplitude is greater than the BPOR baseline amplitude for Baker motor electrical signature analysis data.

Observations

This research was primarily concerned with the proof of concept that motor electrical signature analysis was able to detect motor rotor mechanical faults. During the testing a few observations were noted:

1. The motor rotor rotation must be verified prior to commencing the test.
2. The motor rotor must be balanced in two planes prior to testing.

The motor rotation was not checked prior to the first set of Baker Instrument test runs. This caused the motor current to be substantially lower than was found during the PdMA testing. The Electrician supporting the testing noted the error, and testing started over. During the second run of the test, the motor load was the same as in the PdMA test.

The motor was not balanced in two planes in the beginning of the PdMA testing. Subsequently, the vibration readings were very high at the start of the test. The motor had to be balanced a second time to remove a couple imbalance.

Fan Cowling Data

Although the fan cowling data did pick up the imbalance data, the change in amplitude would have gone unnoticed in a vibration trending program. The amplitude of the vibration values would not have raised concern. With the null hypothesis rejected for

the imbalance, CPSES will re-evaluate the imbalance spectra for vane-axial fans and trend the value in the future.

The fan cowling data did not statistically identify changes in the amplitude of the bearing fault frequencies, which was the purpose of embarking on this research. With the confirmation that the cowling data did not "see" the bearing faulted conditions and the low levels of imbalance, a method of determining faulted fan rotating system is needed.

Fan Bearing Housing Data

The fan bearing housing data was used as a baseline reference to ensure that the faults were measurable and identifiable. Both the inboard and outboard bearing housing readings statistically identified imbalance and bearing faults in the motor outboard bearing. The reference (baseline) data used for comparing the faulted data is considered a standard method of fault detection in the vibration industry (Berry, 1994).

Motor Electrical Signature Analysis

Both of the Motor Electrical Signature Analysis technologies were statistically able to identify a change in the eccentricity (imbalance) of the rotating system. The detection of bearing faults was statistically proven, but the levels of changes were so slight that it will necessitate further investigation into the best methodology for implementing MESA for bearing fault detection.

Stress Wave Analysis

This technology was not part of the statistical test for this research, but the technology is able to detect bearing faults both on the bearing cap and on the fan cowling. Where the vibration data could only see the close coupled data, the stress wave system could “see” the effects of a bearing fault on the fan cowling.

The stress wave system did not detect the eccentricity of the fan. This was not expected and will require further investigation to determine why imbalance was not detected.

CHAPTER 5

CONCLUSION

The purpose of this research was to determine if Motor Electrical Signature Analysis (MESA) would detect Vane-Axial fan degradation. Specifically it detects imbalance, rolling element bearing inner race defects, and rolling element bearing outer race defects. Another purpose of this research was to determine statistically if fan cowling vibration data would detect Vane-Axial fan degradation.

Analysis of the research data resulted in a failure to reject the null hypothesis in all but one instance. The one instance that the null hypothesis was accepted was the fan cowling vibration data for imbalance. The results were very close to equal for the paired comparison test. It was concluded from the analysis that this research can claim that Motor Electrical Signature Analysis can detect Vane-Axial fan degradation. The research does not support the ability of the fan cowling vibration data to detect Vane-Axial fan degradation.

The MESA ability to detect degradation was statistically proven. However, the severity of the degradation, and a standard or metric to determine the extent of degradation was not correlated to the bearing housing vibration condition standards. For this research, a proof of concept, the direct relationship of the MESA data to the vibration data was not attempted due to the complexity of relating the air gap permeability to bearing casing vibration standards.

The research into direct relationship was attempted by Georgia Tech and was determined to vary machine to machine based on the air gap concentricity and permeability for each motor rotor system (Riley, ET. AL., 1997). Therefore, my research focused on the ability of these systems to detect a change in amplitudes at a specific frequency of concern for a given rotor fault instead of a direct comparison to vibration data.

The change in a specific frequency amplitude has practical applications in monitoring the condition of rotating equipment associated with three phase induction motors. The rolling element bearings generate different frequencies depending on the type of failure mode of the bearing. These frequencies are always present, but do not change unless the physical system changes (i.e. lubrication, surface defect, age, or load changes) (Berry, 1994). The imbalance of the motor and alignment is also frequency dependent, and the frequencies for imbalance and alignment are present in the MESA signals. These frequencies, once identified, can be monitored for changes and if analysis does not eliminate a fault or significant change, the motor rotor system's condition can be ascertained.

Finally, it can be concluded that MESA can detect the three types of rotor faults that were introduced in this research. The fan cowling data was not able to detect bearing faults, and was very close to the noise floor in detecting the imbalance. This suggests that MESA could be implemented to trend the specific fault frequencies of a hard to access Vane-Axial fan motor, and monitor for changes that could be detrimental to the operation of the fan system.

RECOMMENDATIONS

From this research, it is concluded that the Motor Electrical Signature Analysis is able to detect the faults that were installed in the fan. This method of motor rotating fault detection should be reviewed for implementation as a part of condition based maintenance practices. The ability to detect Vane-Axial fan mechanical faults has a very low success rate in the utility industry (EPRI, 1998). Nevertheless, since this research was focused on one type of application, Vane-Axial fans, and only three fault types, further research is needed to expand the envelope of fault types and detection using MESA. Since this was a proof of concept for a specific application, the technology may or may not transfer to other equipment system driven with an induction motor.

The research was based on detection of bearings that were artificially degraded and would cause motor or fan damage if left in operation. The purpose of condition based maintenance is to detect faults before equipment failure and to help plan for work on the equipment in a planned and non-impactive way. Since this research looked at essentially failed bearings, research should be carried out with incrementally degraded bearing fault by increasing the severity until the MESA systems detection envelope is obtained.

In addition, even though the stress wave analysis system was not a part of this research, the ability of the system to detect bearing fault should be statistically investigated for bearing fault detection in other applications within the utility industry.

APPENDIX A

DATA COLLECTION

RECORDS

Appendix A
Data Collection
Records

DATA COLLECTION

1. **Prerequisites:**

    a. Verify Motor Data:

Manufacture	Baldore
Horse Power	5
Voltage	460
Full Load Amps	6.4
RPM	1778
Service Factor	1.15
Insulation Class	f code J
Temperature Continuous Operation	40 ºC
Bearings – Inboard	SKF - 6206
Bearings – Outboard	SKF - 6205

2. **Bench Mark Base Line Run #1**
3. **Bench Imbalance Run #1**
4. **Bench Mark Damaged Inner Race Run #1**
5. **Bench Mark Damaged Outer Race Run #1**
6. **Bench Mark Baseline Run #2**
7. **Bench Imbalance Run #2**
8. **Bench Mark Damaged Inner Race Run**
9. **Bench Mark Damaged Outer Race Run #2**

Appendix A
Data Collection
Records

Vane-axial Fan

Data Collection Entry Sheet

1. Verify the prerequisite steps have been completed.

2. Check / verify all the signals at the data collection systems are active.

3. Record the test run: Section: PdMA.

4. Perform the setup activities for next test run.

5. Check / verify each channel of data collection is active and has good signal.

Location	Transducer	Transducer Direction	Component Direction	Amplifier Channel	ADRE Channel
Cowling – Fan End (Inboard)	TU-6123	X	Vertical FIV	1	2
"	"	Y	Axial FIA	2	--
"	"	Z	Horizontal FIH	3	1
Cowling – Free End (Outboard)	TU-6121	X	Vertical FOV	4	4
"	"	Y	Axial FOA	5	--
"	"	Z	Horizontal FOH	6	3
Motor - Fan End (Inboard)	TU-6145	Y	Axial MIA	7	--
"	"	Z	Horizontal MIH	8	5
Motor – Free End (Outboard)	TU-6126	Y	Axial MOA	9	--
"	"	Z	Horizontal MOH	10	7
Motor - Fan End (Inboard)	TU-6692	Z	Vertical MIV	11	6
Motor – Free End (Outboard)	TU-6091	Z	Vertical MOV	12	8

6. Start the fan motor and record the following information: Vibration and PdMA

Measurement	**Value**	**Date**	**Time**	**Notes**	
Temperature	57.5º F	11/26/01	10:00	PdMA data set – took 6 sets of data the first 3 sets the shaft was not balanced.	
Humidity	65%				
Voltage	483				
Inrush Current	33amps				
Running Current	5.3 amps				
Approx. % Load	80%				
Teac Tape Data		**Start** $_{o}$	**Stop** $_{1}$	**Tape**$_{1}$	**Notes**
Run T_1	Tape R_1	10:00:57	10:14:03	13:02	Run #1 unbalanced
Run T_2	"	11:15:00	11:34:00	07:49	Run #2 unbalanced
Run T_3	"	11:43:00	11:54:00	10:55	Run #3 8 grams @ 200º
Run T_4	"	14:58:00	15:05:00	07:22	Run #4 balanced
Run T_5	"	15:07:30	15:15:10	07:37	Run #5, 7.4 g @ 200º
Run T_6	"	16:04:00	16:50:00	10:56	Run #6, balanced w/ BPIR defect

7. Start the fan motor and record the following information: Vibration and PdMA

Measurement	**Value**	**Date**	**Time**	**Notes**	
Temperature	68º F	12/03/01	10:00	Baker data sets took sets of data the first 3 sets the shaft was not balanced. (found out on run # 9 that the fan was running backwards) Run # 10 was a repeat of #9 but in correct direction.	
Humidity	50%				
Voltage	483				
Inrush Current	20 amps				
Running Current	2.3 amps				
Approx. % Load	50%				
Teac Tape Data		**Start** $_{o}$	**Stop** $_{1}$	**Tape**$_{1}$	**Notes**
Run T_7	Tape R_1	11:10:46	11:24:04	13:29	Run #7 balanced
Run T_8	"	13:16:01	13:24:37	07:42	Run #8 7.4 g @ 200º
Run T_9	"	14:26:17	14:40:10	13:56	Run # 9 BPIR Inboard
Run T_{10}	"	15:24:14	15:33:00	08:46	Run #10 BPOR Inboard
Run T_{11}	"	15:46:30	15:57:30	10:56	Run #11 BPOR forward

8. Start the fan motor and record the following information: Vibration and PdMA

Measurement	**Value**	**Date**	**Time**	**Notes**	
Temperature	71º F	12/04/01	09:00	Baker and SWANTECH rebuilt motor to balanced and good bearings, verified rotation. Tape R_1 ran out about 3-4 minutes into the run, took DataPAC information from live run.	
Humidity	90%				
Voltage	483				
Inrush Current	33 amps				
Running Current	3.8 amps				
Approx. % Load	78%				
Teac Tape Data		**Start** $_o$	**Stop** $_1$	**Tape**$_{1\&2}$	**Notes**
Run T_{12}	Tape R_1	09:10:00	**	**	Run #12 – balanced
Run T_{13}	Tape R_2	09:44:55	09:51:58	07:01	Run #13 7.4 g @ 200º
Run T_{14}	"	10:19:35	10:27:30	08:13	Run #14 balanced BPOR

** Tape stopped in the middle of the run.

8. Record the file names / record information for each technology in test:

PdMA File	Run T_1	Run T_2	Run T_3	Run T_4	Run T_5	Run T_6	Run T_7	Run T_8	Run T_9	Run T_{10}	Run T_{11}	Run T_{12}	Run T_{13}	Run T_{14}
unbalanced	**X**													
unbalanced		**X**												
8.0 g 200º			**X**											
Balanced				**X**										
7.4 g 200º					**X**									
BPIR (MOB)						**X**								
Baker File														
Balanced (BW)							**X**							
7.4 g 200º (BW)								**X**						
BPIR (MOB) (BW)									**X**					
BPOR (MOB) (BW)										**X**				
BPOR (MOB) (CR)											**X**			
Balanced												**X**		
7.4 g 200º													**X**	
BPOR														**X**
SWANTECH														
Balanced												**X**		
7.4 g 200º													**X**	
BPOR														**X**

10. Return fan to stowage status:

APPENDIX B

Fan Bearing
Information

SKF

Motor Outboard Bearing – 6205
Motor Inboard Bearing – 6206

Appendix B
Fan Bearing
Information

The following Bearing Frequencies are from SKF and Entek (a Rockwell Automation Company). The formulas are from the Shock and Vibration Handbook.

$$Inner\ Race\ (BPFI) = \frac{n}{2} f\left(1 + \frac{Bd}{Pd} Cos b\right)$$

$$Outer\ Race\ (BPFO) = \frac{n}{2} f\left(1 - \frac{Bd}{Pd} Cos b\right)$$

$$Inner\ Race\ (BSF) = \frac{Bp}{2Bd} f\left[1 - \left(\frac{Bd}{Pd} Cos b\right)^2\right]$$

$$Cage\ (FTF) = \frac{1}{2} f\left(1 - \frac{Bd}{Pd} Cos b\right)$$

b = *Contact Angle*
n = *Number of Balls*
Pd = *Pitch Diameter*
Bd = *Ball Diameter*
fr = *frequency rotation (Hz or CPM)*

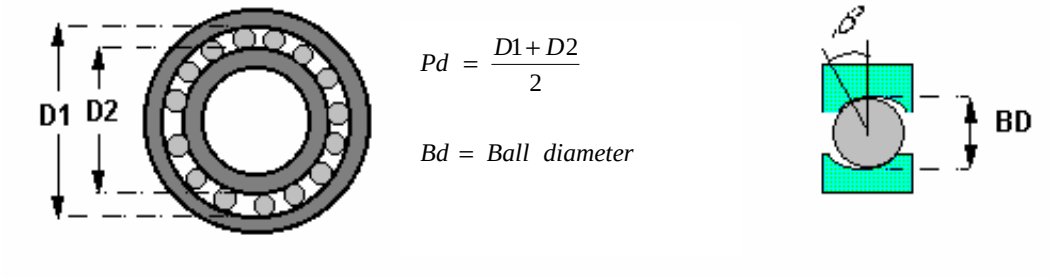

From Brüel & Kjær

Appendix B
Fan Bearing
Information

Table B1 – Bearing Frequencies for Comparison Testing.

Description	Label	Frequency (CPM)	Orders
Speed Reference	1X (running speed)	1772.2	1
Motor Outboard	FTF	703.92	0.3972
Motor Outboard	BSF	4115.1	2.322
Motor Outboard	2xBSF	8230.1	4.644
Motor Outboard	BPOR	6337.4	3.576
Motor Outboard	BPIR	10463	5.904
Motor Inboard	FTF	701.79	0.396
Motor Inboard	BSF	4093.8	2.31
Motor Inboard	2xBSF	8187.6	4.62
Motor Inboard	BPOR	6326.8	3.57
Motor Inboard	BPIR	9623.1	5.43

Approximations:

BPFI = (Nb/2 +1.2) or BPFI => 60% x rpm x # of balls

BPFO = (Nb/2 – 1.2) or BPFO => 40% x rpm x # of balls

BSF = (Nb/2 –1.2/Nb)

FTF = (1/2 – 1.2/Nb)

APPENDIX C

Stress Wave Analysis

SWANTECH

Appendix C
SWANTECH data

DEMONSTRATION OVERVIEW

DATE:

December 4, 2001

LOCATION:

TXU Electric, Comanche Peak

ATTENDEES:

TXU

Donald Doan – Principal Nuclear Technologist: Vibration, Sound and Modal Analysis

SWANTECH

Brian Rucker – Regional Manager
8676 West W Avenue
Schoolcraft, MI 49087
(616) 679-3030
brucker@swantech.com

Brad Cartwright – Sr. Applications Engineer
6682 NW 16th Terrace
Ft. Lauderdale, FL 33309
(954) 975-2212
bcartwright@swantech.com

PURPOSE OF DEMONSTRATION:

To demonstrate SWAN's ability to detect and differentiate a healthy bearing from one with an induced fault.

DEMONSTRATION MACHINERY:

Axial Vane fan

SENSOR LOCATIONS:

Sensor 101	Motor Bearing
Sensor 102	Outer Case

SWANVIEW™ TOOLS:

This section introduces SWANView's three primary tools, Stress Wave Energy (SWE), Stress Wave Amplitude Histograms and Stress Wave Spectral Analysis, which are used to determine the operating characteristics of the demonstration machinery. The analysis in the following pages consists of looking at data from each sensor location in the following manner:

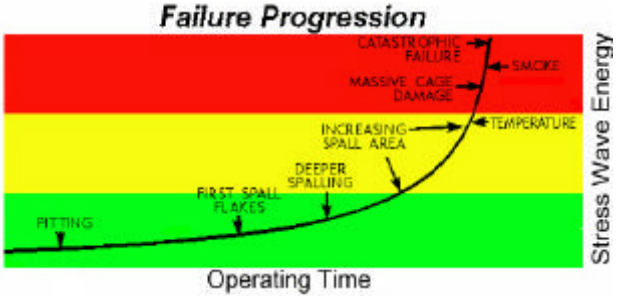

1. Created Operating History Charts capturing data during routine Operation. The Operating Histories trend SWE readings over time and shows them against the backdrop of the green, yellow and red health indicating color zones. The result being an easy-to-interpret graphical representation of the health trend of the machine.
2. Examined the Stress Wave Amplitude Histogram (SWAH) to determine whether the distribution was normal (bell shaped) and at the lower end of the amplitude scale (x-axis). This tool takes each individual sensor output-voltage reading (sampled at 20,000 readings per second) and distributes them into voltage-bins that correspond to the value of each reading. In healthy machinery, the distribution should be a narrow bell shape (because the voltage readings are consistent, thus distributed over a narrow voltage range) and at the lower end of the voltage scale (because minimal abnormalities are present to excite the sensor to higher amplitudes). As aperiodic events occur (usually the result of lubrication problems such as fluid or particulate contamination or skidding between rolling elements), the voltage readings occur over a much broader range at a higher amplitude. The result is a much broader distribution that is shifted to the right on the voltage scale (x-axis).
3. Examined the Stress Wave Spectra for spectral lines more than 10 dB above background levels. SWAN sensors only detect events capable of exciting the sensor at 40,000 Hz. All the normal machine dynamics are filtered out and what remains is a time history of shock or friction modulating events. In healthy machinery, a minimal number of shock events occur thus the spectral analysis yields only a relatively flat horizontal line with no significant

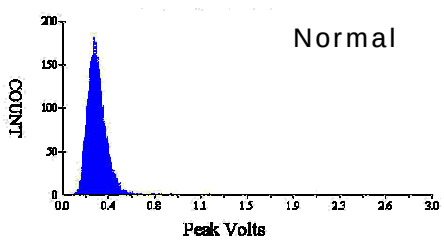

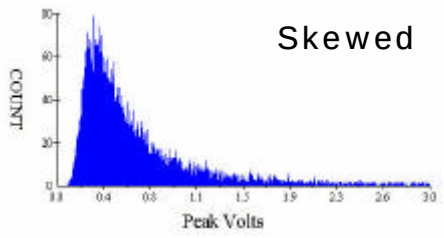

spectral lines (spikes in the vertical direction). When a damage zone is present, a repetitive shock event occurs as the damage zone makes contact with mating parts. This repetitive shock event shows up in the spectral analysis as a spectral line (spike) at the frequency that it occurs. When a spike does occur, the geometry of the rolling elements and the speed at which they are rotating can be analyzed to determine the precise part that could cause shock at that frequency, thus indicating the damaged component and its location.

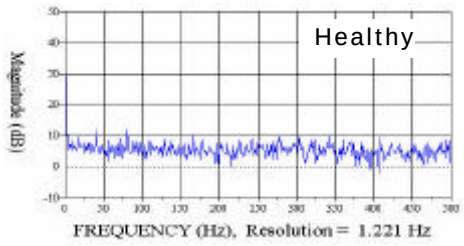

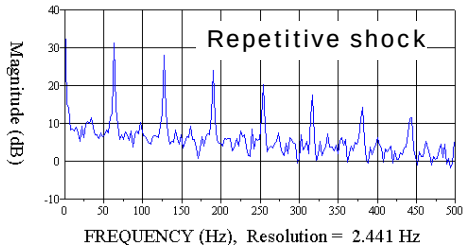

DATA AND RESULTS

The EPRI Seeded Fault Bearing test demonstrates how Stress Wave Analysis quickly and easily differentiates a healthy component from a damaged one in a clear and unambiguous manner. SWAN confirmed healthy operation of an electric fan motor known to be good while showing a dramatic difference in the unit when a fault was induced. SWAN's Stress Wave Energy Index increased by over 375% from the healthy condition to the damaged condition, an unmistakable indicator. In addition, both SWAN's Histogram and Spectral Analysis clearly differentiate the damaged unit from the normal.

An unbalance was induced on the fan for a brief period to test another technology's ability to detect this condition. SWAN sensors were connected to the unit during this phase of testing and did not detect the unbalance. SWAN is very effective at detecting unbalance conditions in machinery, although it is only detectable when it is severe enough to overload the

bearing. In this case, the 4-gram unbalance was not enough to adversely affect the bearing's performance; therefore SWAN did not detect it.

Machinery of varying degradation is easily diagnosed and differentiated with the SWAN System, as the data that follows will show. The data is also presented in an easy to interpret graphical display that enables a user to determine the health of a machine or component within a matter of minutes with minimal training.

The thresholds on the health-indicating color zones were set using the undamaged bearing as a guide to what the nominal amount of friction would be from a healthy unit. In reality, a comprehensive configuration would include data from multiple machines. A key characteristic of SWAN technology is friction levels between like machines operating in a healthy condition are very similar. Thus a unique baseline need not be set on every machine. One properly established baseline can be used to immediately verify whether any like machine is operating in a healthy state or not, significantly reducing the time, resources and data compilation required by other conventional condition monitoring methods.

STRESS WAVE ENERGY

Stress Wave Energy is an excellent indication of the overall health of a machine because it is a direct measurement and comparison of the amount of friction and impacting occurring. The charts on Page 4 show the Stress Wave Energy trends for the Normal, Unbalanced and Seeded Fault Bearing condition from both the Motor Bearing and Outer Case sensor locations. The Seeded Fault Bearing is unmistakable as compared to both the Normal and Unbalanced conditions. The Normal operating condition is characterized by a very linear data trend,

completely horizontal and steady with very little variance. Contrast this to the Seeded Fault condition where the data trends 350% higher than the Normal condition, well into the Yellow and even the Red health indicating color zone. Note too the erratic nature of the trend as compared to the very steady trend from the healthy condition. This is unmistakable evidence of an undesirable operating condition that even the most novice analyst can discern.

Data from the Outer Case sensor location reacts identical to the Motor Bearing location although the Stress Wave Energy values are considerably less. This is due to the sound path restrictions from the bearing to the outer case where the sensor was mounted. Several mechanical interfaces (including the epoxy required to affix the sensor mount) and thin support structures obstructed the bearing from the sensor location. Regardless, this location was still an effective location for differentiating the Normal from the Damaged condition.

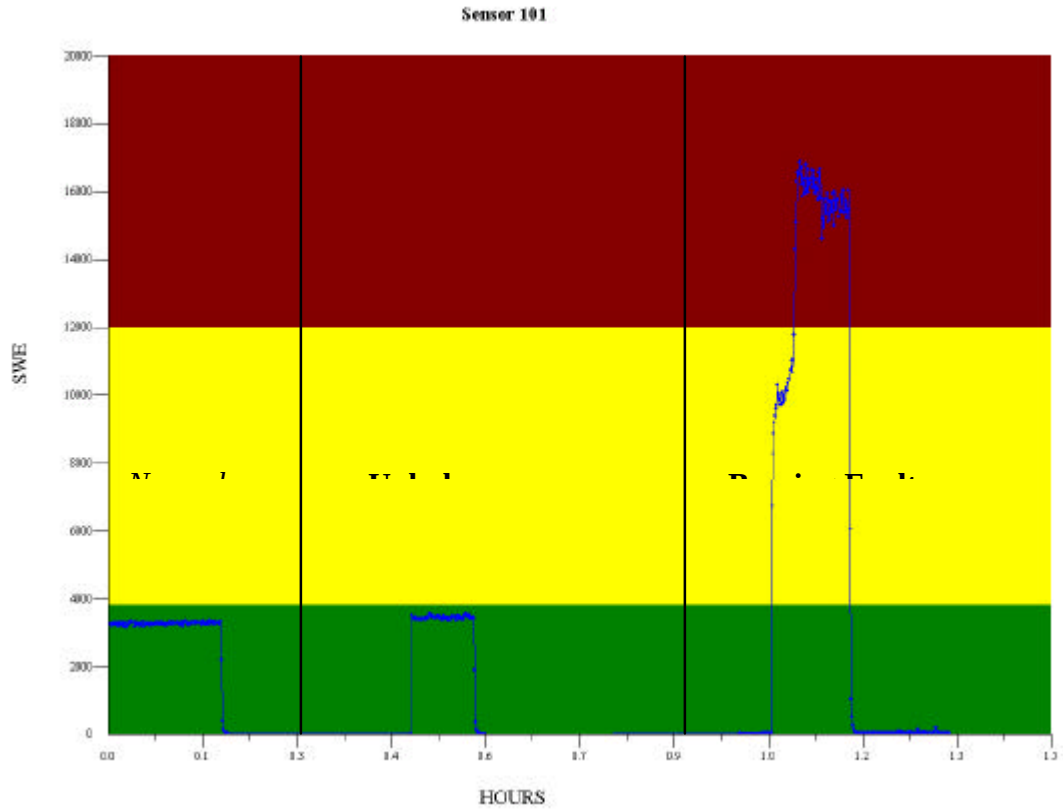

Stress Wave Energy: Motor Bearing Sensor

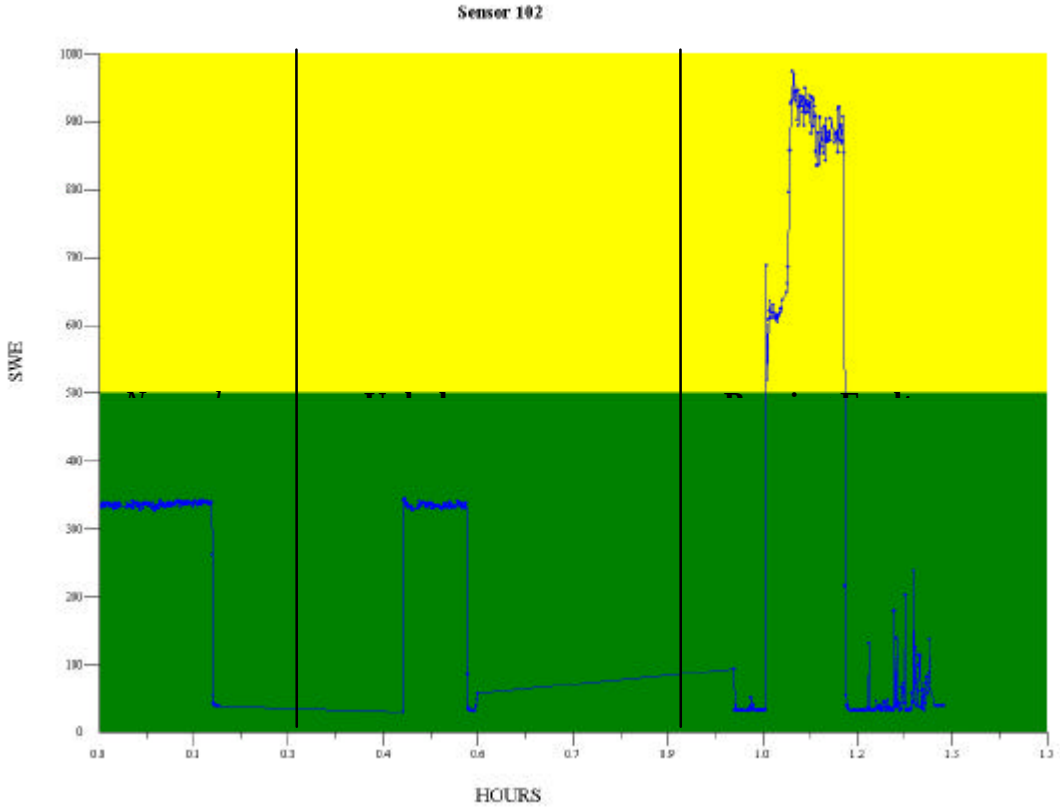

Stress Wave Energy: Outer Case Sensor

STRESS WAVE HISTOGRAM

The Histogram is an excellent tool for measuring the consistency of a machine. Of importance in the histogram is the shape of the distribution. A normal bell shaped curve with minimal "tailing" to the right on the x-axis is a sign of a well lubricated, consistent system. A broad-based distribution with excessive tailing to the right on the x-axis shows poor lubrication effectiveness. Potential causes of a skewed Histogram could be particulate or fluid contamination, skidding events, sliding contact or rubbing.

The Histogram from the 'Normal Bearing' from each sensor location (Page 5 & 6 - Top) offer excellent examples of how consistent, healthy operation manifests itself with this tool. The very narrow-based gasussian (normal, bell shaped) distribution implies very little variance in the bearing performance and good lubrication effectiveness. Note too that the distribution is shifted all the way to the left on the amplitude scale (mean voltage of 0.74 volts) showing that a minimal amount of excitation of the sensor is occurring.

In stark contrast to the Normal Bearing, the 'Seeded Fault Bearing' (Page 5 & 6 - Bottom) yields a histogram with classic signs of abnormal, aperiodic shock events; precisely what is expected from contamination of lubrication that results when metallic particles have been evacuated from the races. Notice the much broader distribution shifted to the right on the amplitude scale (mean voltage of 2.25 volts). This alone shows that the Seeded Fault Bearing is much more stressed than the Normal Bearing. The key indicator in this histogram however is the excessive skewing (tailing to the right) Exceeding 6 Volts on the x-axis. This is classic evidence of particulate contamination as would be expected from a damaged bearing. It was confirmed that particles from the induced bearing fault remained inside of the bearing.

In addition, during the Seeded Fault run, Stress Wave Energy can be seen taking a big upwards step from the Yellow Zone into the Red Zone on the Motor Bearing sensor location (see Page 4 – Top). This is strong evidence of a sizable particle breaking from the bearing and becoming ground up in the bearing - another contributor to a skewed histogram.

Histogram: Motor Sensor

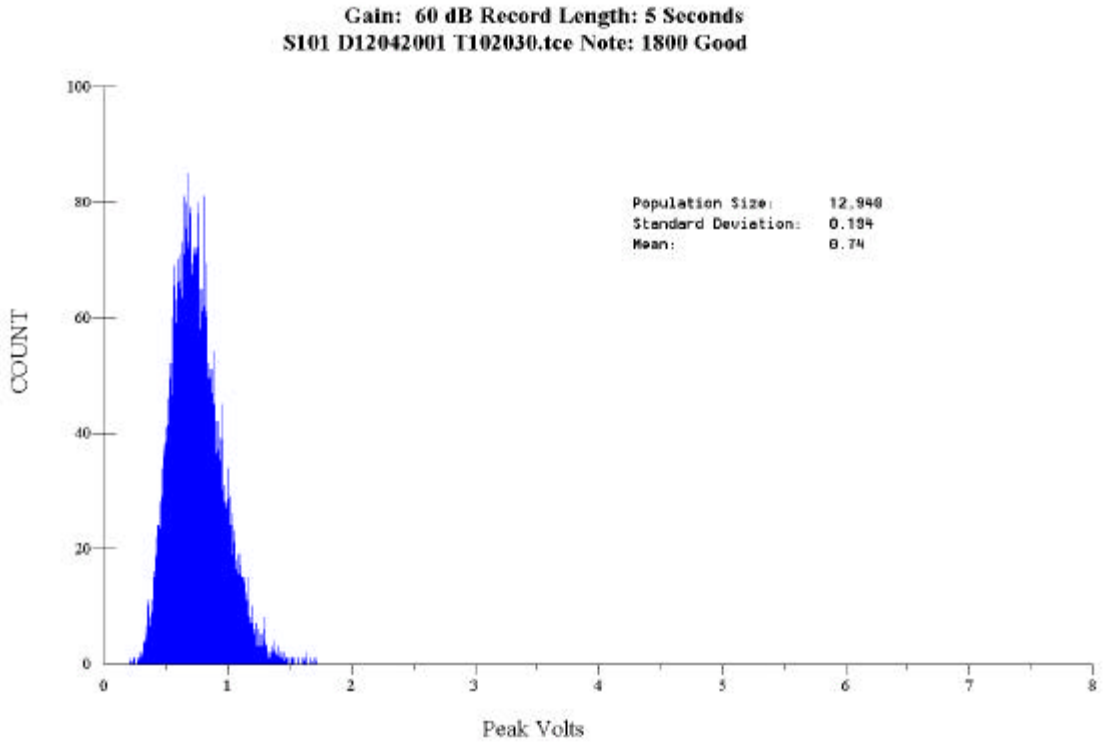

Normal Bearing

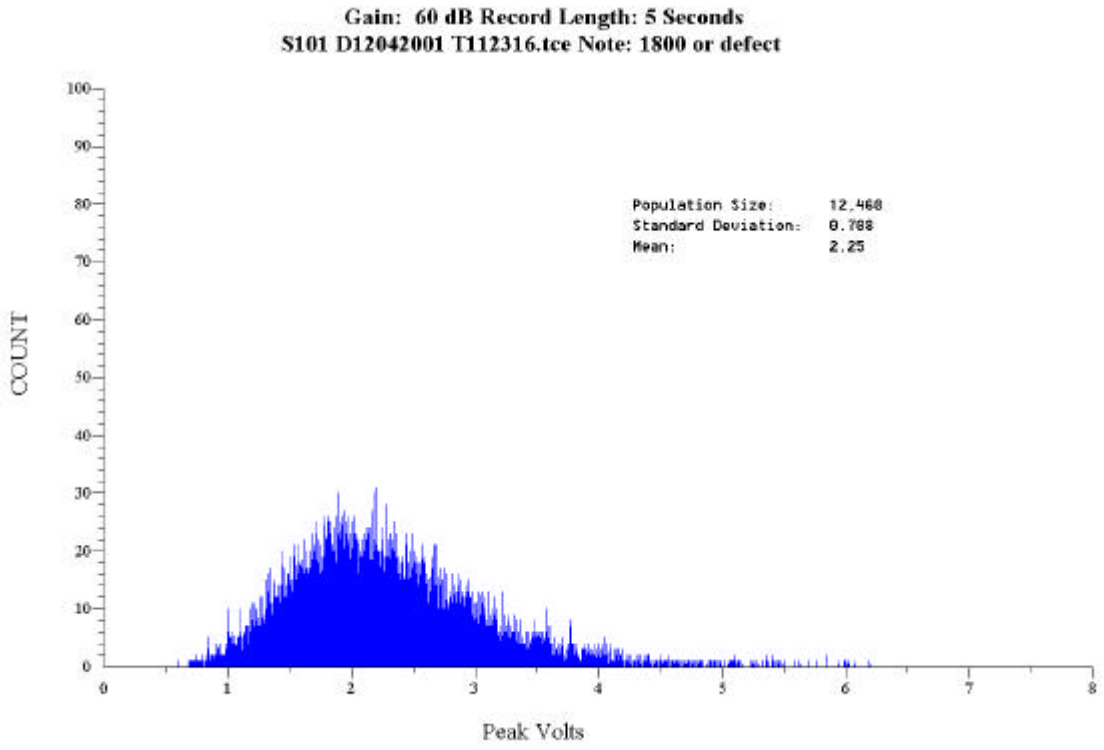

Seeded Fault Bearing

Histogram: Outer Case Sensor

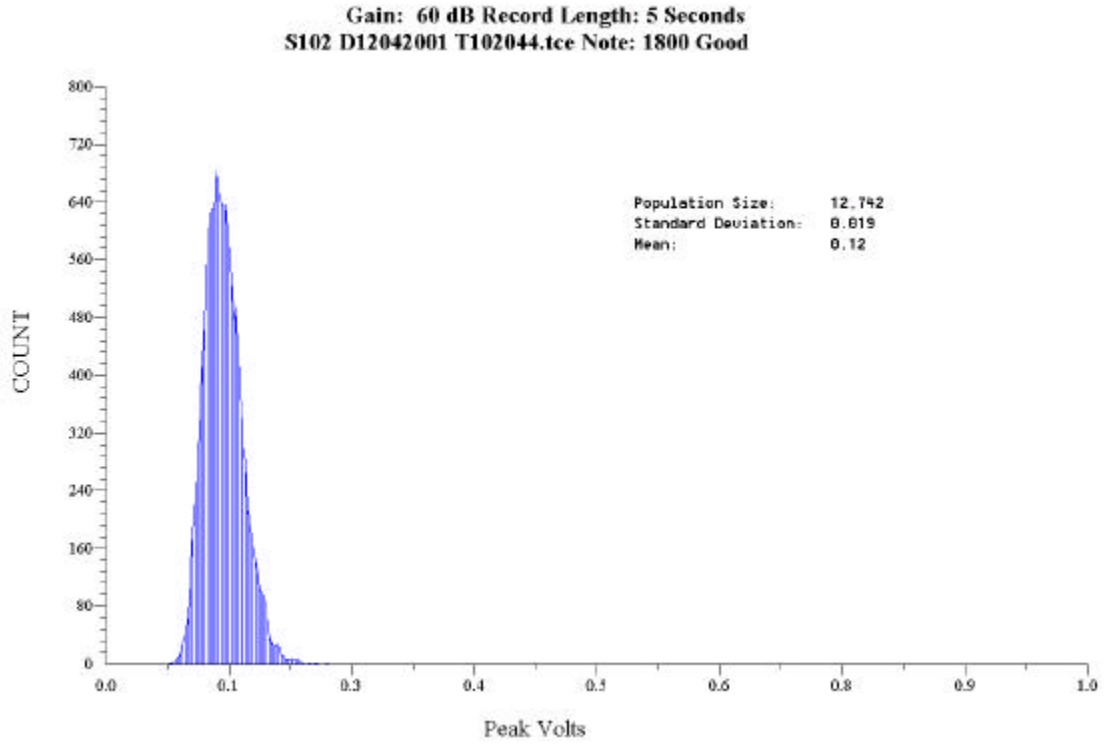

Good Bearing

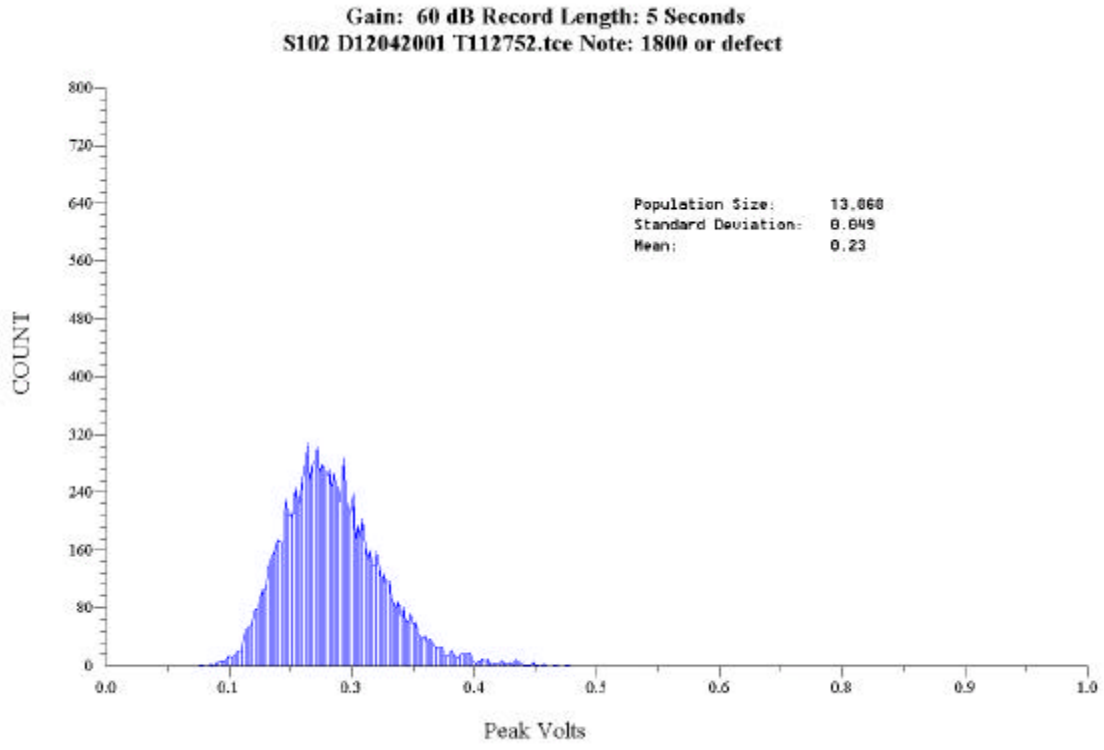

Seeded Fault Bearing 101: Motor Bottom

Appendix C
SWANTECH data

STRESS WAVE SPECTRAL ANALYSIS

SWAN's spectral analysis tool is ideal for isolating damage to dynamic components. Quite simply, a flat spectrum verifies that no repetitive shock events typical of bearing or gear damage are occurring. On the other hand, a spectrum with a significant spectral line or lines (a spike in the vertical direction) at least 10 dB above background levels indicates a repetitive friction or shock event at that frequency. Readily available bearing and gear data assist in identifying the machine components that could potentially cause a shock event at a particular frequency

The difference between a healthy bearing and a damaged bearing are clearly shown with the Stress Wave Spectral Analysis tool. The Spectral Analysis plots from both the Motor Bearing and Outer Case sensor locations (Pages 8 & 9) show clear differences from the Normal Bearing to the Seeded Fault Bearing. The Normal condition produces a very flat spectrum with a single peak at 106.2 Hz, the outer race defect frequency. A single peak as such indicates that there is in fact a minor disturbance in friction at the outer race of the bearing, perhaps light false brinelling. Without harmonics, it is certainly not an impacting event or significant disturbance.

Contrast this to the Seeded Fault condition where numerous peaks at 106.2 Hz multiples (harmonics) are seen. In addition, an abundance of peaks at 11.6 Hz, the Fundamental Train Frequency (cage) are present. This conclusively shows that a significant impacting event at 106.2 Hz, the outer race, is occurring during the Seeded Fault condition. Since the induced fault was damage to the outer race, this data confirms that the excessive increase in Stress Wave Energy during the Seeded Fault run (see Page 4) was in fact the result of the induced outer race damage.

Stress Wave Spectrum: Motor Sensor

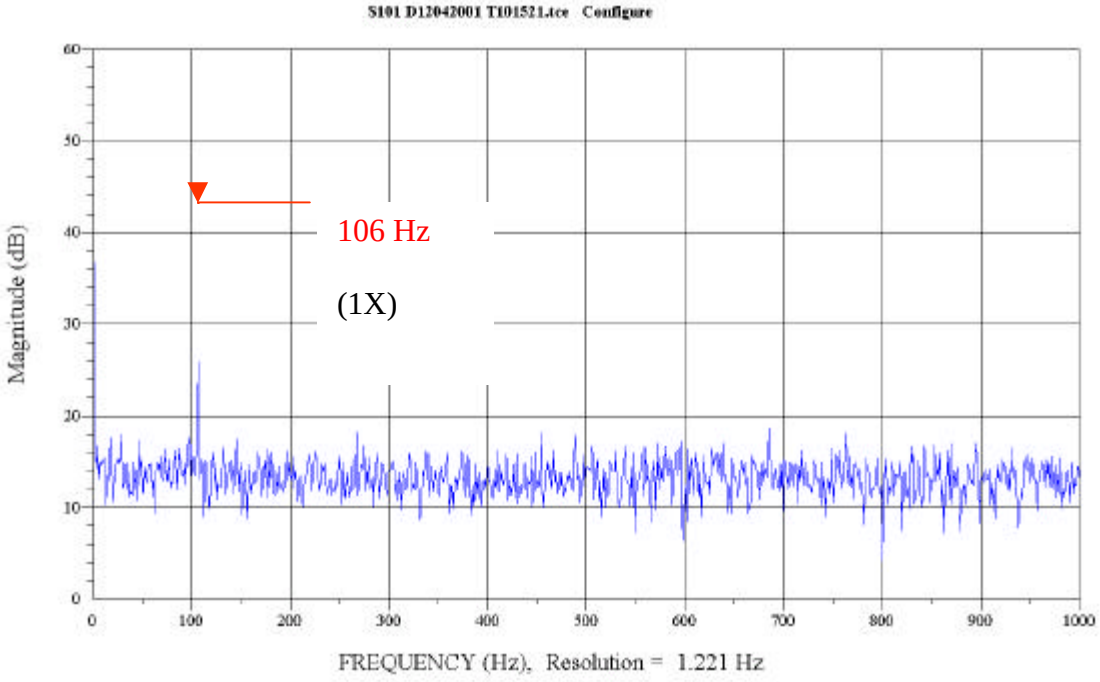

Normal Bearing

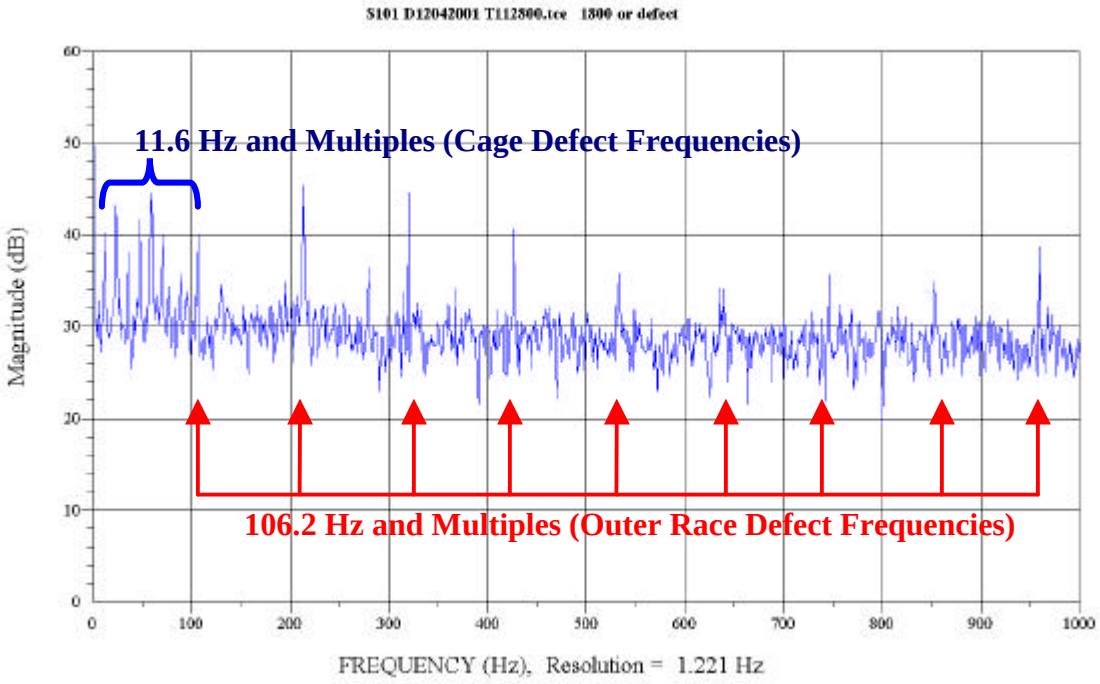

Seeded Fault Bearing

Stress Wave Spectrum: Outer Case Sensor

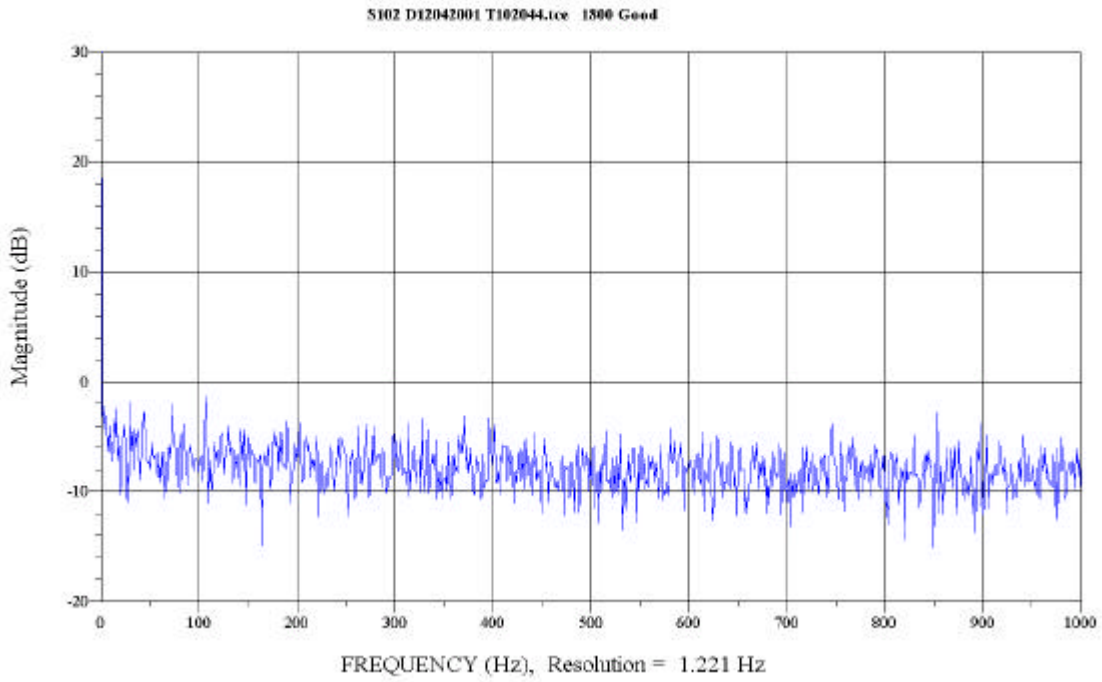

Normal Bearing

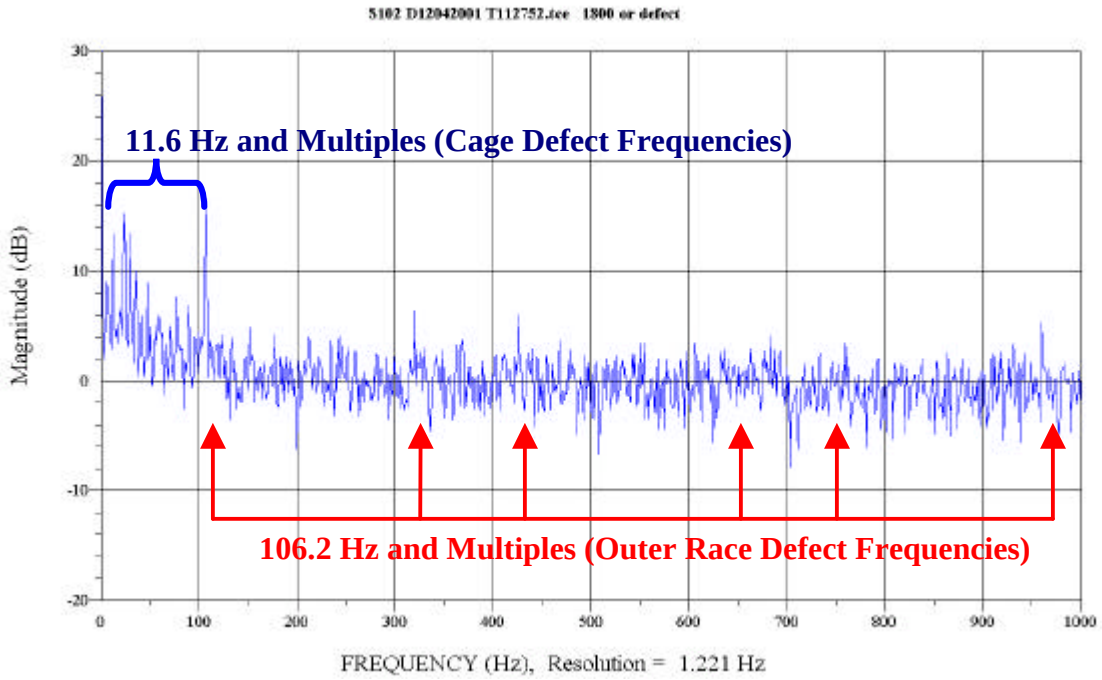

Seeded Fault Bearing

CONCLUSIONS

The EPRI demonstration on the Axial Vane Fan shows that SWAN provides a degree of resolution into the operating condition of machinery previously unattainable with traditional diagnostic methods. The differences between healthy and damaged machinery components are displayed in a clear and unambiguous manner allowing even the most inexperienced analysts to differentiate damaged from healthy operation – even in the early stages of a failure.

SWAN technology is second to none at not only detecting, but also trending the progression of damage levels in machinery. The results on the Axial Vane Fan are a perfect example of this. SWAN's Stress Wave Energy measurement, a first line of defense measuring the overall health of a machine, showed unmistakable evidence that Seeded Fault Condition represented an undesirable operating condition that required immediate attention. The trends in the high Yellow (and even Red) Health indicating color zones illustrate this in an unambiguous manner. These values are 300-400% greater than the levels experienced during the Normal Bearing runs.

Once the presence of damage is verified with the Stress Wave Energy readings, SWAN's additional tools are used to isolate the source of the damage. In the case of the Seeded Fault Bearing, SWAN's Histogram tool clearly shows excessive randomly occurring friction events. High Stress Wave Energy coupled with a broad based, skewed histogram confirms that the unit is operating with particulate contamination as a result of the induced fault.

SWAN's Spectral Analysis tool also detected clear evidence of impacting at the outer race and cage of the bearing during the Seeded Fault run. The abundance of spectral lines from the Seeded Fault run at the outer race and cage frequencies confirms that the increases in Stress Wave Energy are a direct result of the induced bearing damage.

The SWAN System was specifically designed to support engineering and maintenance efforts by providing the information you need to do your job smarter and faster. The system is flexible and has been proven in numerous aerospace, propulsion, industrial and turbine applications. No other technology offers the simplicity of use and the superior level of fault detection accuracy that is provided by the SWAN System.

Appendix C
SWANTECH data

COMPANY PROFILE

SWANTECH, LLC designs, manufactures, and markets advanced condition-monitoring products used to determine the health of operating machinery. Our patented Stress Wave Analysis (SWAN™) technology provides early and quantifiable detection of defects and incorporates sophisticated diagnostic tools and artificial intelligence capabilities to provide true predictive maintenance. SWAN products make it possible to determine the existence of machine defects, identify which components are affected by the defect, and provides the opportunity to correct the problem prior to the occurrence of secondary damage or catastrophic machine failure. As a maintenance tool, SWAN products can be used to improve machinery efficiency, reduce operating expenses, and protect the customer's investment in their heavy machinery.

SWANTECH's corporate headquarters, including design engineering, manufacturing and test facilities are located in Fort Lauderdale Florida, USA. A facility in Orlando, FL provides additional design engineering services, test facilities and quick response manufacturing capabilities for prototyping and system integration.

SWANTECH is the market expert in the development and application of Stress Wave Analysis technology. This technology, along with SWAN diagnostic tools, provides the vital data needed to minimize downtime, optimize production and effectively allocate personnel resources.

SWANTECH's exciting new technology has performed successfully in a wide variety of applications including:

Gas Turbine Engines for Electric Power Generation
Critical Airport Drive Motors for the FAA
Marine Generators and Propulsion Equipment Aboard Navy and Commercial Ships
Complex Paper Mill Machinery
Gearbox Equipment in a Rolling Mill
Rotating Components on Metro-Rail Cars for the Miami-Dade Mass Transit System
F/A-18 Airframe Mounted Gearbox
C-130 Engine Gearbox
H-60 Helicopter Gearbox
Axial Fan Blower Bearings
Automotive Transmissions
SWAN was recently used to successfully detect and differentiate various types of Foreign Object Damage (FOD) in a seeded fault test at a major aircraft engine manufacturer.

Appendix C
SWANTECH data

SWANTECH is dedicated to staying in the forefront of the design and development of advanced monitoring and predictive maintenance tools that increase machinery efficiency and reduce maintenance and product loss costs.

Once the presence of damage is verified with the Stress Wave Energy readings, SWAN's additional tools are used to isolate the source of the damage. In Carnival's case, SWAN's Histogram tool clearly shows excessive randomly occurring friction events from Air Conditioner Unit 4's Motor, Non-Drive Bearing. High Stress Wave Energy coupled with a broad based, skewed histogram confirms this. The good bearings on the other hand have low Stress Wave Energy and normally distributed histograms. SWAN's Spectral Analysis confirms no localized surface damage to the bearings. The damage is in the form of uniform wear, which eventually progresses to localized damage.

The true benefit of the SWAN system comes from comparative data taken over the course of time. The system becomes even more valuable as more data is collected and the Health Indicating Color Zones are fine-tuned. With this repository of information, subtle changes become recognizable as abnormal conditions. These capabilities enable SWAN to provide the information needed to better understand the affects of manipulating test conditions in the test cell environment.

The SWAN System was specifically designed to support maintenance efforts by providing the information you need to do your job smarter and faster. The system is flexible and has been proven in numerous aerospace, propulsion, industrial and turbine applications. No other technology offers the simplicity of use and the superior level of fault detection accuracy that is provided by the SWAN System.

What is Stress Wave Analysis (SWAN)?

Stress Wave Analysis (SWAN) technology represents over 25 years of research and development in the application of high frequency acoustic diagnostic techniques. SWAN enables the separation of stress waves from the much lower frequency range of operating machinery vibration and audible noise. This innovative technology enables true predictive maintenance for rotating and reciprocating machinery.

Reliable condition monitoring requires maintenance personnel to be able to identify machine defects at early stages and be able to monitor the progression of the defect. At its earliest stages, a defect will not cause any significant loss in machine operating efficiency. Through continued operation, the defect will increase and become a potential source of secondary damage.

As machine parts come in contact with the defect, even at the earliest stages, shock and friction events generate ultrasound or Stress Wave Energy (SWE).

Stress Wave Analysis (SWAN) detects and measures this energy and damage levels well below the levels required to excite vibration sensors, and before sufficient damage has occurred to activate metal chip detectors in lubrication systems.

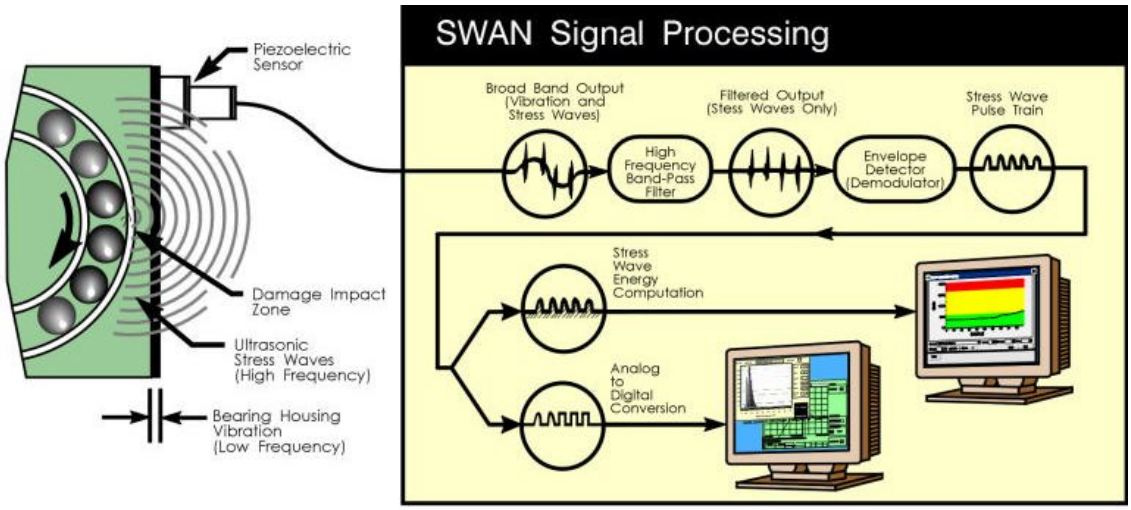

A sensor firmly mounted on the structure detects stress waves, transmitted through the machine's structure. A piezoelectric crystal in the sensor converts the stress wave energy into an electrical signal which is then amplified and filtered by a high frequency band pass filter in the analog signal conditioner to remove unwanted low frequency sound and vibration energy.

The output of the signal conditioner is a Stress Wave Pulse Train (SWPT) that represents a time history of individual shock and friction events in the machine. The digital processor then analyzes the SWPT to determine the peak level of the SWE and the total energy content

generated by the shock event. The computed SWE is displayed on the system's control panel or monitor and can be recorded with other SWE readings.

SWAN measures even slight shock and friction events that occur between contact surfaces. The level and pattern of anomalous shock events becomes a diagnostic tool.

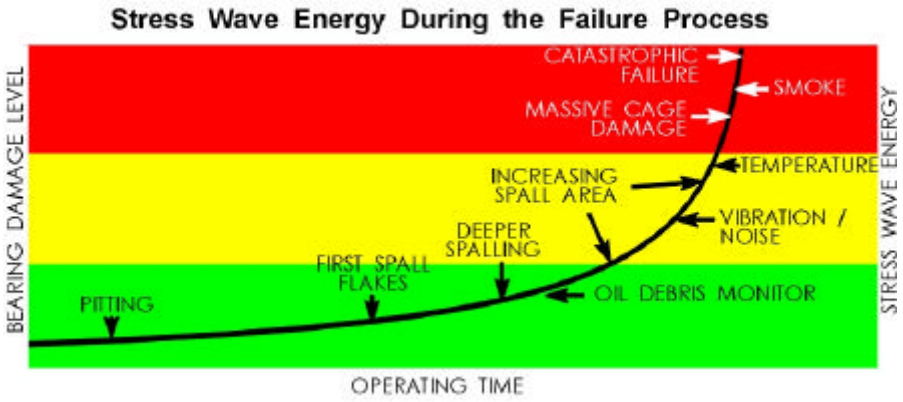

THE FAILURE PROCESS

Regardless of when failures occur during a machine's life cycle, they start as small discrepancies and progress to larger ones that result in secondary damage, unacceptable operating conditions, or catastrophic failure. Traditional diagnostic techniques do not provide a clear indication of problems until late in the failure process. SWAN Stress Wave Energy (SWE) measurements provide a *QUANTITATIVE* measure of internally generated shock and friction energy during the entire life cycle of a machine. SWE is trendable throughout the failure process from its earliest stages to an unacceptable operating condition. The trend of SWE measurements from normal levels through caution and danger zones provides the information necessary for advance scheduling of corrective action, and true predictive maintenance.

Failure rate is a function of operating time, as shown in the classical bathtub curve. The probability of failure is larger during initial hours of machine operation, but quickly decreases to a constant rate. Improper assembly, installation error, improper run-in, and rough shipping and handling conditions all contribute to this period of infant mortality (stage 1). Abnormal levels of SWE associated with infant mortality failure modes can be detected and corrective action taken during the acceptance testing. By monitoring the equipment early in its life cycle, unforeseen failures can be avoided and normal baseline levels set for monitoring the machine's condition during the remainder of its useful life.

The second and third stages of a machine's life cycle are periods characterized by a constant, but relatively low, probability of failure. For many critical pieces of rotating machinery, the time at which the probability of wear out failure begins is not known. This is because operating time or cycle limits are established for overhaul of the equipment prior to wear out. These overhaul limits are set conservatively in an effort to prevent increasing rates of unforeseen critical equipment failure. The quantitative nature and predictive accuracy of SWE, as a measure of

machine condition, allows the Time Between Overhauls (TBO) to be safely extended to the time when wear out begins (stage 4). The benefits of this service life extension are not only economic, but operational as well. These operational benefits include both reduced downtime for equipment replacement/overhaul and reduced overall failure rates (by deferring the reoccurrence of infant mortality failures in newly installed/overhauled machines).

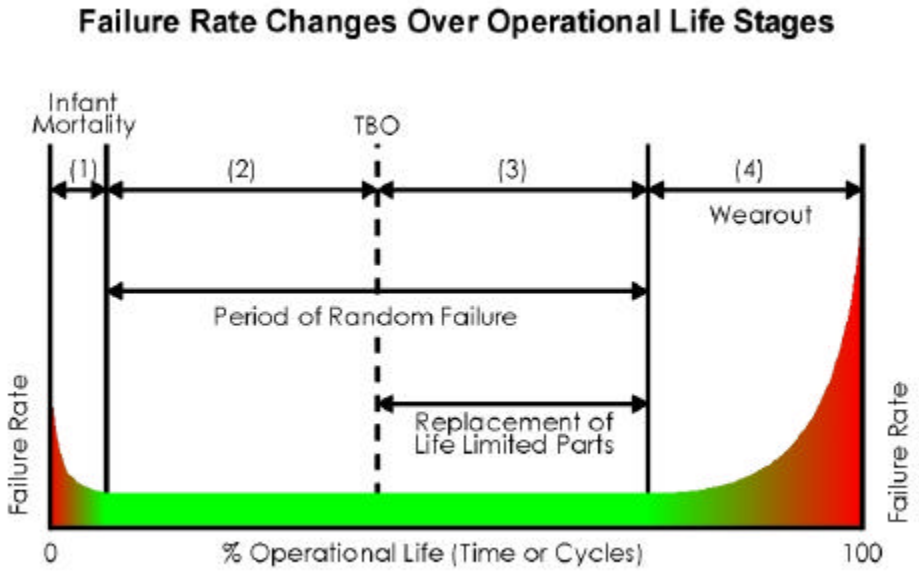

The time at which a machine enters the wear out phase of its life cycle is a function of its inherent design reliability and its operation history. Thus different individual machines in a population of identical machines may begin to wear out at different times. The predictive maintenance capability provided by SWAN allows every machine to be operated for as long as its failure rate can be maintained at acceptable levels through preventative maintenance and minor repairs. When it becomes necessary to operate a machine into the final stage of its life cycle, SWAN is essential to provide advance notice of impending failure.

The SWAN system provides early problem detection and enables maintenance professionals to track the progression of damage through acceptable levels of wear. The trending data provided by SWAN could be used to determine the probability of failure and even to determine the machine parts that are affected by the damage. This information is vital in the scheduling of pro-active maintenance and implementation of corrective action with minimal impact to machinery operation.

SWAN Product Engineering is focused on standards-based solutions and packaging to ensure interoperability with other vendor systems. SWAN's System Architecture & Platforms are easily expandable to monitor multiple locations and allow integration with other diagnostic systems.

APPENDIX D

Transducers & Meter and Test Equipment

Appendix D
Transducers &
Meter and Test Equipment

The following table lists the manufacture, serial number, calibration, and engineering units used for this research.

Manufacture	Serial Number	Calibration Due	Units	Location	Comments
PCB	TU-6103	09/12/02	100 mV/g	Cowling Inboard X	Tri-axial
PCB	TU-6104	09/12/02	100 mV/g	Cowling Outboard Y	Tri-axial
PCB	TU-6105	09/12/02	100 mV/g	Motor Inboard X	Tri-axial
PCB	TU-6106	09/12/02	100 mV/g	Motor Inboard Y	Tri-axial
PCB	TU-6107	09/12/02	100 mV/g	Motor Inboard Y	Tri-axial
PCB	TU-6108	09/12/02	100 mV/g	Motor Inboard Y	Tri-axial
PCB	TU-1440	06/20/02	Voltage	All Channels	PCB 12 Channel Power Supply
Bently Nevada	TU-1380	06/22/02	Vibration Units	All Channels	8 Channel Data Acquisition Instrument
Entek IRD	TU-1704	12/03/02	RPM	Fan Shaft	Laser Tachometer

All calibrations are done at TXU Electric, CPSES Metrology Lab and the calibrations are traced to National Standards:

ANSI / NCSL Z-540-1-1994, American National Standards for Calibration

IEEE Standard 498-1985, Requirements for calibration and control of measurement and test equipment

ISO/IEC 17025, General requirements for the competence of testing and calibration laboratories

REFERENCES

Baxter, N. 2001, Interview by author, 13 November 2001. Notes. Glen Rose, Texas: Autor.

Bechard, P. 2001, *EMAX Demodulation,* Motor Reliability Technical Conference, May 2001.

Berry J. E. 1993, *Predictive Maintenance and Vibration Signature Analysis I*. Columbus, Ohio, IRD Mechanalysis, Inc.

Berry J. E. 1994, *Predictive Maintenance and Vibration Signature Analysis II*. Columbus, Ohio, IRD Mechanalysis, Inc.

Bethel, N.P. 2001, *The Developing role of Current Analysis in Predictive Maintenance,* P/PM Technology, August 2001 P/PM Technology.

Brown, C.T. 2001, Interview by author, 12 November 2001. Notes. Glen Rose, Texas: Autor.

Casada D.A. 1998, *Using Motor Data to Improve System Reliability and Reduce Operating Costs*, Oakridge National Laboratories: lecture series

Casada D.A. 1999, *Using an electric motor as a Transducer to: monitor centrifugal pump (and other ancillary equipment) conditions*, Oakridge National Laboratories: lecture series

Casada,D.A. 2001, Interview by author, 9 November. Notes. Glen Rose, Texas: Author.

Diamond, S.J. 1989, *Practical Experiment Designs (for Engineering and Scientists),* New York, Van Norstrand Reinhold

EPRI, 1991*Power Plant Electrical Reference Volume 6*, EPRI, December 1991: 6-7 – 6-11. Palo Alto, Ca: Research Reports Center

Frarey, J. L. 1995, *Machinery Vibration Analysis III Course*, Vibration Institute, 1995

Gastonal, B. 2001, Interview by author, 12 November 2001. Notes. Glen Rose, Texas: Author.

General Installation, *Operation and Maintenance Instructions for Aerovent Products*, Aerovent, IM-100, September 1996.

Gökmem Burak, Eldem Vasfi, Duyar Ahmet, 2001, MCM : *A New Technology in Predictive Maintenance*, Paper from conference at Oak Ridge National Laborites, 2001.

Harris C. M. 1988, *Shock and Vibration Handbook*: ed. Harold B. Crawford and David E. Fogarty: R.R. Donnelley & Sons Company, McGraw Hill USA.

Hinton P.R. 1999, *Statistics Explained*: New York, NY Routledge

Mitchell J. S. 1993, *Machinery Analysis and Monitoring*: pg – pg. Tulsa, Oklahoma: PennWell Books.

Riley, C.M., Lin, B.K., Haberler, T.G., Schoen, R.R., 1997, *A Method for Sensorless On-Line Vibration Monitoring of Induction Machines*, IEEE Paper

Rosen J. 2001, Wireless Sensor Array Project @ Exelon Limeric Generating station, EPRI.

SKF 1995, *Bearing Handbook*, San Diego, CA. SKF press

Sternstein, Martin, 1996, *Statistics*, Hauppauge, NY. Barron's.

Taylor, J.I. 1994, *The Vibration Analysis Handbook.* Tampa, FL: Vibration Consultants

Wiedenbrug, E. J. 1999, *Measurement Analysis and Efficiency Estimation of Three Phase Induction Machines Using Instantaneous Electrical Quantities.* Rochester, NY: Applied Image Inc.

Wiedenbrug, E.J. 2001, *Instantaneous Torque as Predictive maintenance Tool for Variable Frequency Drives and Line Operated Motors*, Paper by Baker Instrumentation Company

Wiedenburg, E.J., Wallace, A. *Motor Efficiency Determination: From Testing Laboratory to Plant Installation*, IEEE Paper

Wiedenburg, E.J., Wallace, A. *Induction Machine Speed Extraction by Analysis of Stator Current Signatures'*, IEEE Paper

Wiedenburg, E.J., Wallace, A., von Jouanne, A., 1997, *Using the New EPRI/BPA Testing Facility to Evaluate the Latest Technologies in Motors and Drivers*, IEEE Paper

Wiedenburg, E.J., Wallace, A., Von Jouanne, A., Douglass, J., 1997, *A Laboratory Assessment of In-Service Motor Efficiency Testing Methods*, IEEE Paper

Wiedenburg, E.J., Wallace, A., Von Jouanne, A., Andrews, P.S., 1997, *The Measured Effects of Under-Voltage, Over-Voltage and Unbalanced Voltage on the Efficiency and Power Factor of Induction Motors over Wind Ranges of Load*, IEEE Paper

Wiedenburg, E.J., Ramme A., Matheson E., von Jouanne, A., Wallace, A. 2001. *Modern on-line testing of Induction Motors for Predictive Maintenance and Monitoring,* Paper by Baker Instrumentation Company and Oregon State University.

Wowk, Victor, 1991, *Machinery Vibration Measurement and Analysis.* Mexico, McGraw-Hill, Inc.